

Department of Physics, Chemistry and Biology

Master's Thesis

Search for Dark Matter in the Upgraded High Luminosity LHC at CERN

Impact of ATLAS phase II performance on a mono-jet analysis

Sven-Patrik Hallsjö

Thesis work performed at Stockholm University

Linköping, June 4, 2014

LITH-IFM-A-EX--14/2863--SE



**Linköpings universitet
TEKNISKA HÖGSKOLAN**

Department of Physics, Chemistry and Biology
Linköping University
SE-581 83 Linköping, Sweden

Search for Dark Matter in the Upgraded High Luminosity LHC at CERN

Impact of ATLAS phase II performance on a mono-jet analysis

Sven-Patrik Hallsjö

Thesis work performed at Stockholm University

Linköping, June 4, 2014

Supervisor: **Docent Christophe Clément**
 FYSIKUM Stockholm University
Professor Magnus Johansson
 IFM, Linköping University

Examiner: **Professor Magnus Johansson**
 IFM, Linköping University



Avdelning, Institution
Division, Department

Theoretical physics group
Department of Physics, Chemistry and Biology
SE-581 83 Linköping

Datum
Date

2014-06-04

Språk
Language

Svenska/Swedish
 Engelska/English

Rapporttyp
Report category

Licentiatavhandling
 Examensarbete
 C-uppsats
 D-uppsats
 Övrig rapport

ISBN
—

ISRN
LITH-IFM-A-EX--14/2863--SE

Serietitel och serienummer **ISSN**
Title of series, numbering —

URL för elektronisk version

<http://urn.kb.se/resolve?urn=urn:nbn:se:liu:diva-XXXXXX>

Titel Sökandet efter mörk materia i den uppgraderade hög luminositets LHC i CERN
Title Search for Dark Matter in the Upgraded High Luminosity LHC at CERN

Undertitel Påverkan av ATLAS fas II prestanda på en mono-jet analys
Subtitle Impact of ATLAS phase II performance on a mono-jet analysis

Författare Sven-Patrik Hallsjö
Author

Sammanfattning
Abstract

Disclaimer: Abstract not yet completed.

Something as an introduction:

The LHC at CERN is undergoing an upgrade to increase the center of mass energy for the colliding particles which means that new physical processes will be explored. One drawback of this is that it will be harder to isolate unique particle collisions since more and more collisions will occur simultaneously, so called pile-up.

One hope for the upgrade is that WIMP models of dark matter will be detected.

This thesis covers looking at effective operators which try to explain dark matter without adding new theories to the standard model or QFT.

Some results and a slight conclusion.

Nyckelord

Keywords

Disclaimer: This not yet completed., ATLAS, Beyond standard model physics, CERN, Dark matter, Elementary particle physics, High energy physics, something, this is in mythesis.sty

4 **Abstract**

5 **Disclaimer: Abstract not yet completed.**

6 Something as an introduction:

7 The LHC at CERN is undergoing an upgrade to increase the center of mass en-
8 ergy for the colliding particles which means that new physical processes will be
9 explored. One drawback of this is that it will be harder to isolate unique parti-
10 cle collisions since more and more collisions will occur simultaneously, so called
11 pile-up.

12 One hope for the upgrade is that WIMP models of dark matter will be detected.

13 This thesis covers looking at effective operators which try to explain dark matter
14 without adding new theories to the standard model or QFT.

15 Some results and a slight conclusion.

16 **Acknowledgments**

17 [REDACTED]

18 A big thank you to my family, fiancée and friends who have supported me through-
19 out my education. A warm thank you to my friend Joakim Skoog who altered
20 some of the images for me.

21 [REDACTED]

22 [REDACTED]

23 *Linköping, June 2014*
24 *Sven-Patrik Hallsjö*

Contents

Notation

1 Introduction

1.1	Research goals	2
1.2	Theoretical Background	3
1.2.1	Quantum mechanics and quantum field theory	3
1.2.2	Nuclear, particle and subatomic particle physics	4
1.2.3	The standard model of particle physics	4
1.2.4	Dark matter	5
1.2.5	Effective field theory	6
1.2.6	Search for WIMPS	8
1.3	Experimental overview	10
1.3.1	LHC	10
1.3.2	ATLAS	11
1.3.3	Coordinate system	12
1.3.4	Reconstructing data	12
1.3.5	Pile-up	13
1.3.6	Mono-jet analysis	13
1.3.7	Phase II high luminosity upgrade	14
1.3.8	Monte Carlo simulation	15

2 Validation of smearing functions

2.1	Smearing functions	18
2.1.1	Electron and photon	18
2.1.2	Muon	18
2.1.3	Tau	18
2.1.4	Jets	18
2.1.5	Missing Transversal Energy	18
2.2	Validation	20
2.2.1	Method	20
2.3	Results	21
2.3.1	Electron and photon	22
2.3.2	Muon	23

58	2.3.3	Tau	23
59	2.3.4	Jets	24
60	2.3.5	Missing Transversal Energy	25
61	2.4	Expected results	26
62	2.5	Discussion	28
63	2.5.1	Smearing independent on pile-up	28
64	2.5.2	Comparison to expected results	28
65	2.6	Conclusion	29
66	3	Evaluating dark matter signals	31
67	3.1	Signal to background ratio	32
68	3.1.1	Signal Region	32
69	3.1.2	Weight	32
70	3.1.3	Verification of background normalization	32
71	3.1.4	Errors in data	33
72	3.1.5	Figure of merit	33
73	3.1.6	D5 operator models	35
74	3.1.7	Light vector mediator models	35
75	3.2	Signal region definitions	36
76	3.2.1	Signal regions	36
77	3.2.2	Verifying background data	36
78	3.3	Mitigating the effect of the high luminosity	36
79	3.4	Results	37
80	3.4.1	Verifying background data	37
81	3.4.2	Events	37
82	3.4.3	Limit on M^*	39
83	3.4.4	Effect of pile-up on M^*	40
84	3.4.5	Previous results	40
85	3.4.6	Limit on mediator mass	40
86	3.4.7	Effect of pile-up on mediator mass	42
87	3.5	Discussion	43
88	3.5.1	Comparison to previous results	43
89	3.5.2	Effect of the high luminosity	43
90	3.6	Conclusion	44
91	3.6.1	Limit on M^*	44
92	3.6.2	Limit on mediator mass	44
93	4	Results and Conclusions	45
94	4.1	Validation of smearing functions	45
95	4.2	Signal to background ratio	46
96	4.2.1	Limit on M^*	46
97	4.2.2	Limit on mediator mass	46
98	4.3	Other selection criteria and observables	46
99	4.3.1	Limit on M^*	46
100	4.3.2	Limit on mediator mass	46
101	4.4	Mitigating the effect of the high luminosity	46

102	4.5 Recommendations to mitigate the effect of the high luminosity	46
103	4.6 Suggestions for future research	46
104	A Datasets	49
105	A.1 Background processes	49
106	A.1.1 Validation	49
107	A.1.2 Background to signals	49
108	A.2 Signals	50
109	A.2.1 Qcut	50
110	A.2.2 D5 signal processes	50
111	A.2.3 Light vector mediator processes	50
112	Bibliography	55

Notation

NOTATIONS

Notation	Explanation
barn(b)	$1 \text{ barn}(b) = 10^{-24} \text{ cm}^2$
\oplus	$a \oplus b = \sqrt{a^2 + b^2}$, $a \oplus b \oplus c = \sqrt{a^2 + b^2 + c^2}$

ABBREVIATIONS

Abbreviation	Expansion
ATLAS	A large Toroidal LHC ApparatuS
CERN	Organisation européenne pour la recherche nucléaire ¹
CMS	Compact Muon Solenoid
CR	Control Region
LHC	Large Hadron Collider
MC	Monte Carlo
RMS	Root Mean Square
SM	the Standard Model of particle physics
SR	Signal Region
WIMP	Weakly Interacting Massive Particle
WIMPS	Weakly Interacting Massive ParticleS
QED	Quantum ElectroDynamics
QFT	Quantum Field Theory
QM	Quantum Mechanics

¹Originally, Conseil Européen pour la Recherche Nucléaire

1

Introduction

119 Discrepancies in measurements of the rotations of galaxies indicate the presence
120 of a large amount of matter which interacts through gravity, though not elec-
121 tromagnetically making it invisible to our telescopes. This matter is commonly
122 referred to as dark matter. Since no known or hypothesised particle in the stan-
123 dard model of particle physics can be used as a candidate for dark matter, this
124 hints at the presence of new physics.

125 At the Organisation Européene pour la Recherche Nucléaire (CERN) focus now
126 lies to discover any evidence of so called weakly interacting massive particles
127 (WIMPS) which may be a candidate for dark matter. It is usually impossible to
128 detect any interaction of dark matter candidates on the subatomic scale, however
129 through looking at proposed interactions, searching for assumed decay channels
130 and by investigating what is invisible to the detectors by using momentum con-
131 servation it is hoped that signs will be found. Though to date, none have been
132 found.

133 Both experiments and current theories now show that higher energies are re-
134 quired at the LHC to be able to see any signs. This is why the LHC and all detectors
135 are undergoing a vast upgrade program [1]. In this thesis focus will be on the last
136 part of the upgrade due for completion in 2023, known as the high luminosity-
137 LHC phase II upgrade; and also on the ATLAS detector. The method used in this
138 thesis focuses on looking at data which emulate conditions at the upgraded LHC.

139 1.1 Research goals

140 This research took place at Stockholm University from January 7th until **when**?

141 During the research period the following tasks were set up and performed/answered:

- 142 • Implement a C++ programme that loops over the collisions inside the signal
143 and background datasets.
- 144 • For each collision retrieve the relevant observables (variables used to extract
145 the signal over the background) and apply "smearing functions" to emulate
146 the effect of the high luminosity on the observables.
- 147 • For both signal and background datasets, compare observables before and
148 after smearing. What observables are the least/most affected?
- 149 • Implement selection criteria that selects the signal collisions efficiently while
150 reduces significantly the background. In a first step the selection criteria
151 should be taken from existing studies.
- 152 • Selection criteria can be evaluated and compared with each other using a
153 figure of merit P , that measures the sensitivity of the experiment to the dark
154 matter signal. Calculate P for the given selection criteria before and after
155 smearing.
- 156 • What is the effect of the high luminosity (smearing) on the value of P ?
- 157 • Investigate other selection criteria and observables, to mitigate the effect of
158 high luminosity. Use P to rank different criteria after smearing.
- 159 • Conclude on the effect of the high luminosity on the sensitivity for dark matter
160 and possible ways to mitigate its effects using alternative observables
161 and selection criteria.

1.2 Theoretical Background

1.2.1 Quantum mechanics and quantum field theory

In the beginning of the 20th century, some physical phenomena could not be explained by classical physics, for example the ultra-violet disaster of any classical model of black-body radiation, and the photoelectric effect [2]. It was these phenomena that led to the formulation of quantum mechanics (QM), where energy transfer is quantized and particles can act as both waves and particles at the same time [3].

Combining QM with classical electromagnetism proved harder than expected, colliding a photon(em-field) and an electron (particle/wave) is quite tricky. This can be seen when trying to calculate the scattering between them both in a QM schema. One idea that came from this was to explain them both in the same framework, field theory. Also, trying to incorporate special relativity into QM suggested a field description where space-time is described using the metric formalism from differential geometry. The culmination of both of these problems is the first part of a Quantum field theory (QFT), Quantum electrodynamics (QED) which with incredible precision explains electromagnetic phenomena including effects from special relativity[4]. It is in this merging that antimatter was theorised, since it is a requirement for the theory to hold. After the discovery of antimatter, the theory was set in stone. Since this the theory has been altered somewhat to explain more and more experimental data. This is discussed more in subsection 1.2.2 and subsection 1.2.3.

To be able to calculate properties in QFT one uses the Lagrangian formalism [5], which gives a governing equation for the different physical processes. In general the Lagrangian used for the Standard model is quite complicated, one can thus focus on one of the different terms corresponding to a specific interaction. This can be done to calculate the so called cross-section for a process, which is related to the probability that that process will occur. A step to simplify the calculations is to use the so called Feynman diagrams, an example of which is given in figure 1.1.

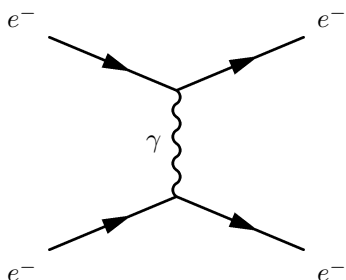


Figure 1.1: An example of a Feynman diagram explaining an electron-electron scattering using QED.

Through the figure, which comes with certain rules, and knowing what the major process (in this case QED) one can calculate the cross-section [4]. It is this that is needed to predict what one will be able to detect new particles.

1.2.2 Nuclear, particle and subatomic particle physics

Many could argue that these branches of physics started after Ernest Rutherford famous gold foil experiment [6], where he discovered that matter is composed of matter with a nucleus, a lot of empty space and electrons.

It was this that sparked the curiosity to see what the nucleus is made of and what forces govern the insides of atoms. After this, and the combination of the theoretical description given by QM, a lot more has been discovered and still more has been predicted. The newest of these is of course the Higgs particle, which was predicted through QFT and then discovered by the ATLAS and the CMS experiments at CERN [7].

The discovered particles are often divided into different groups depending on the fundamental particles that build them up. For instance, particles build up of three quarks are known as hadrons. Particles with an integer spin are known as bosons whereas half-integer particles are known as fermions.

1.2.3 The standard model of particle physics

The standard model of particle physics, referred to simply as the standard model (SM), is the particle zoo which tries to categorize all the particles and that have been discovered experimentally. QFT explains the interactions between these particles and it has also predicted several particles by including symmetries [6]. Regarding SM, Gauge bosons are the force carriers for the different forces, quarks are the and leptons are the fundamental blocks that we know of so far. The difference between the later two is if they interact via the strong force or not.

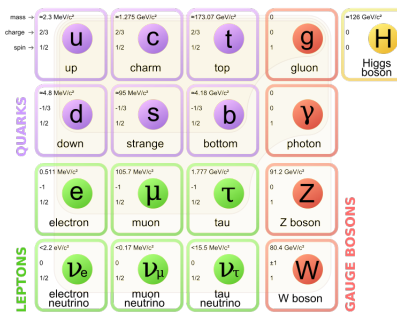


Figure 1.2: The standard model of particle physics where the three first columns represent the so called generations, starting with the first. [8].

SM is today the pinnacle of particle physics and can be used to explain almost everything that occurs around us. There are however some problems [9]:

- There is no link between gravity and the SM.
- Asymmetry between matter and antimatter can not be fully explained.
- No dark matter candidate!
- No explanation that can contain dark matter.

223 In this thesis focus lies with dark matter, some more introduction to possible
 224 dark matter and different candidates in extensions to SM are explained in subsection
 225 1.2.4.

226 1.2.4 Dark matter

227 Dark matter is among other things, the name given to the solution to the discrepancies
 228 of galactic rotations.

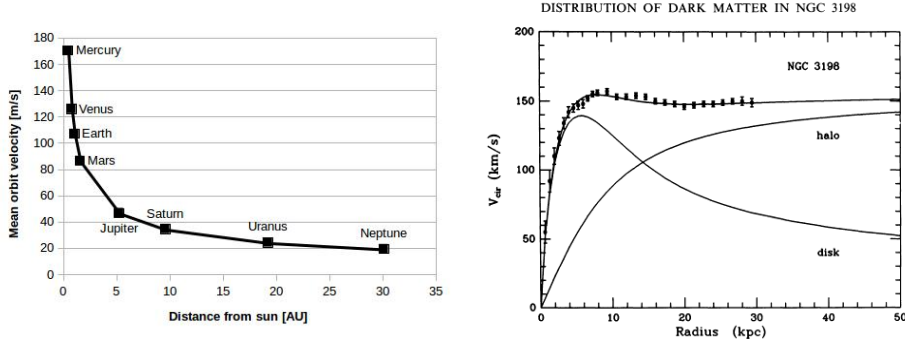
229 To explain this, focus on matter in a galaxy which are rotating around the center
 230 of the galaxy. Through Newtons law of gravity and the centrifugal force one can
 231 calculate the rotation speed dependent on the distance to the center of the galaxy.
 232 Since one of these forces is attractive and the other repulsive, if the matter is in
 233 a stable orbit around the galactic center (which they are) they must be equal and
 234 give us an expression for the speed depending on the distance. Newtons law can
 235 be written as the following:

$$F_{Gravitational} = G \frac{Mm}{r^2} = G_M \frac{m}{r^2} \quad F_{Centrifugal} = m \frac{V^2}{r} \quad (1.1)$$

236 where G is the gravitational constant, M the mass of the centre object, m the mass
 237 of the matter, r the distance between the two and V is the rotation speed. It has
 238 been simplified using G_M since all matter orbits the same galactic center. Setting
 239 the equations in (1.1) results in:

$$G_M \frac{m}{r^2} = m \frac{V^2}{r} \Leftrightarrow V^2 = \frac{G_M}{r} \Rightarrow V = \sqrt{\frac{G_M}{r}} \propto \frac{1}{\sqrt{r}} \quad (1.2)$$

240 where the speed is assumed to be positive and \propto means proportional. Through
 241 these simple calculations it shown that the rotation speed should decrease with
 242 and increased distance. The same reasoning can be applied to our solar system
 243 where this is the case figure 1.3a. The relation in these units is $V = \frac{107}{\sqrt{r}}$ where
 244 107 can be used in (1.2) to calculate the mass of the sun. However when looking
 245 at galaxies, even when taking into account that one has to see the galaxies as a
 246 mass distribution and that the above is only true when outside of the inner mass
 247 half, this is not the case! In figure 1.3b experimental data can be seen from the
 248 galaxy NGC3198 with a fitted curve which does not decrease with the distance
 249 but is instead constant. This is the discrepancy which is solved by postulating
 250 the existence of dark matter. After this the big question arises, what could this
 251 dark matter consist of? What is known so far lies in the name. It is called dark
 252 since there is no electromagnetic interaction and matter since it has gravitational
 253 interaction. This means that it can not be made up of any baryonic matter or
 254 anything in the Standard Model apart from neutrinos. The main interest of this
 255 thesis and also the main contributor to the rotational discrepancies is known as
 256 cold dark matter. This is due to the matter having a low speed, thus low kinetic
 257 energy, and have a high particle mass (In the GeV scale) [9, 12, 13]. This means
 258 however that neutrinos can not be a candidate, thus dark matter can not be made
 259 out of any standard model particles. There are several ideas to detected dark
 260 matter, [9]



(a) *Rotation speed of planets in our solar system. Since the distance is quite small on an astronomical scale, there is no sign of dark matter. Based on data from [10].*

(b) *Rotation speed of matter in NGC3198 with a curve fitting and three different models, if only a dark model halo existed, if there was no dark matter and the correct, if both exist [11].*

Figure 1.3: Different rotation curves, both for planets in our solar system and matter in the NGC3198 galaxy.

- Ordinary matter interacting with ordinary matter can produce dark matter, known as production. Which is the processes that occurs at particle accelerators.
- Dark matter interacting with ordinary matter can produce dark matter, known as direct detection.
- Dark matter interacting with dark matter can produce ordinary matter, known as indirect detection.

In this thesis the focus lies with production. There are several theories how to detect dark matter in proton-proton collisions such that occur at the LHC at CERN this is covered more in subsection 1.2.6.

1.2.5 Effective field theory

In quantum field theory the objective is usually to find the part of the Lagrangian which explains a type of interaction, known as the operator of the interaction and also to find the probability amplitude (cross-section) for a certain interaction. For complicated processes it is easier to employ certain conditions so that the small scale phenomena are simplified and the whole picture understood. This is known as using an effective field theory and the concept is explained in figure 1.4. The operator can be found through assuming the possible interactions and using the effective field theory [4]. The cross-sections can be found through the Feynman diagrams as described in subsection 1.2.1.

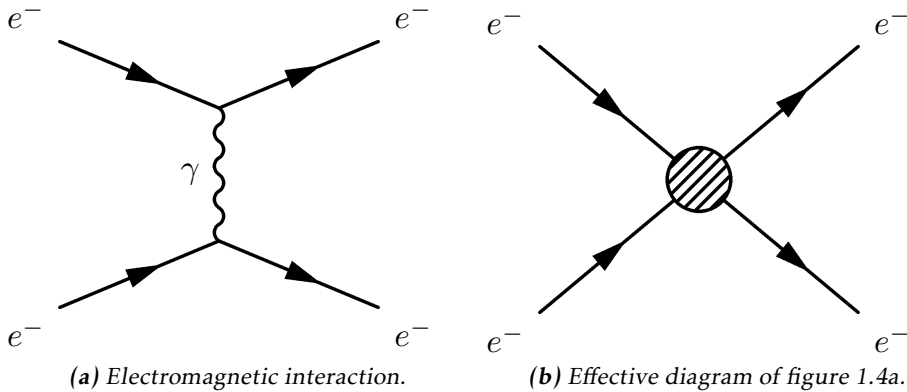


Figure 1.4: Feynman diagram of an electron-electron scattering, both as an ordinary diagram and as its effective theory version, where the details are hidden in the blob.

In this thesis the same effective field theory as in Refs. [12, 14] will be considered. The WIMP (usually denoted χ) is assumed to be the only particle in addition to the standard model fields. It is assumed that an even number of χ must be in every coupling. It is assumed that the mediator exists is heavier than the WIMPS, meaning that their interactions are in higher order terms of the effective field theory and thus not included in the operators. For simplicity, the WIMPS are assumed to be SM singlets, thus invariant under SM gauge transformations, and the coupling to the Higgs boson is neglected.

The operators used in this thesis are assumed to be quark bilinear operators on the form $\bar{q}\Gamma q$ where Γ is a 4×4 matrix of the complete set,

$$\Gamma = \{1, \gamma^5, \gamma^\mu, \gamma^\mu \gamma^5, \sigma^{\mu\nu}\} \quad (1.3)$$

This will dictate how the operators are written, more of why this is done can be found in [4, 12, 14].

This defines an effective field theory of the interaction of singlet WIMPs with hadronic matter. It is an approximation which will break down when the mediator mass is close to the mass of the WIMP. The condition for this is derived in [14] and gives:

$$M > 2m_\chi \quad (1.4)$$

where m_χ is the mass of the WIMP and M is the mass of the mediator particle. There is also the requirement that:

$$M \lesssim 4\pi M_* \quad (1.5)$$

where M_* is the energy scale where the effective theory is no longer a good approximation.

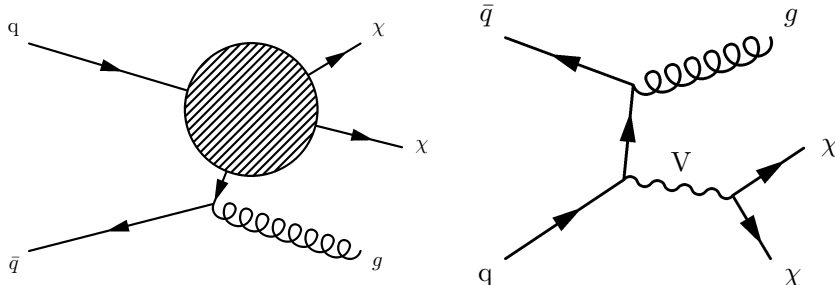
301 In this work, WIMPS are assumed to be Dirac fermions (half integer spin and is
 302 not its own antiparticle).

303 In table 1.1 the operators which are integrated out via the effective field theory
 304 and are of interest in this thesis are given.

Name	Initial state	Type	Operator
D1	qq	scalar	$\frac{m_q}{M_*^3} \bar{\chi} \chi \bar{q} q$
D5	qq	vector	$\frac{1}{M_*^2} \bar{\chi} \gamma^\mu \chi \bar{q} \gamma_\mu q$
D8	qq	axial-vector	$\frac{1}{M_*^2} \bar{\chi} \gamma^\mu \gamma^5 \chi \bar{q} \gamma_\mu \gamma^5 q$
D9	qq	tensor	$\frac{1}{M_*^2} \bar{\chi} \sigma^{\mu\nu} \chi \bar{q} \sigma_{\mu\nu} q$
D11	gg	scalar	$\frac{1}{4M_*^3} \bar{\chi} \chi \alpha_s (G_{\mu\nu}^a)^2$

Table 1.1: Table based on discussion in [13].

305 Where D denotes that the WIMPS are assumed to be Dirac fermions. These can all
 306 be described using figure 1.5a.



(a) Effective Feynman diagram explaining the D-operators. **(b)** Feynman diagram describing the vector mediator model.

Figure 1.5: Feynman diagrams describing the signal models used in this thesis.

307 Another model which is considered is a vector mediator model which is described
 308 by figure 1.5b.

309 1.2.6 Search for WIMPS

310 The search for WIMPS is based on a mono-jet analysis which is described in sub-
 311 section 1.3.6. This method revolves around a high energetic jet which arises from
 312 the gluon from figure 1.5b and momentum missing from the energy conservation.

313 This means that something has happened which the detectors can not detect. If
314 the models from subsection 1.2.5 can explain the missing energy, then a model
315 for WIMPS has been found.

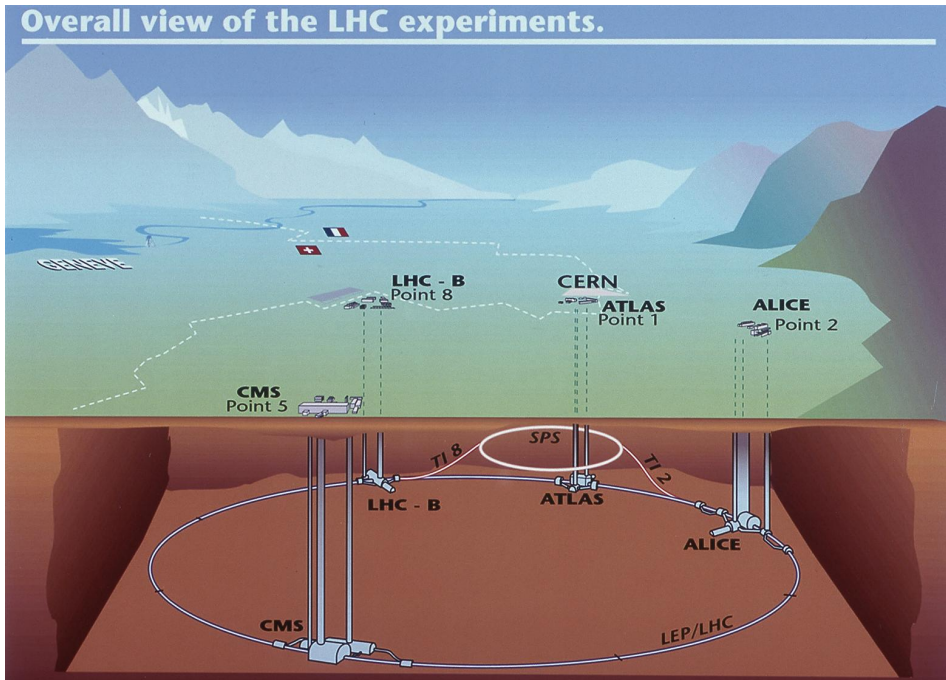
316 Since the search for WIMPS at the LHC is based on looking at the missing energy,
317 not actual detection, the experiment can not establish if a WIMP is stable on a
318 cosmological time scale and thus if it is a dark matter candidate [13]. This means
319 that if a candidate is found, it may still not be the dark matter that is needed to
320 explain the cosmological observations.

321 The different theories discussed in subsection 1.2.5 require some process in which
322 quarks and anti-quarks are produced. At ATLAS they have looked at proton-
323 proton collisions, in which they are produced, with 8 TeV center of mass energy
324 with out finding any excess of mono-jet events. This is why it is very interesting
325 that the LHC is undergoing a upgrade that will allow higher energy levels, see
326 subsection 1.3.7. With this the processes can be given higher energy and thus the
327 produced particles can be comprised of higher mass.

328 1.3 Experimental overview

329 1.3.1 LHC

330 The large hadron collider (LHC) is a particle accelerator located at CERN near
 331 Geneva in Switzerland, see figure 1.6. The accelerator was built to explore physics
 332 beyond the standard model and to make more accurate measurements of stan-
 333 dard model physics. Before it was shut down for an upgrade in 2012 it was able
 334 to accelerate two proton beams to such a velocity that each proton in them had
 335 an energy of 4 TeV which gives a center of mass energy, $\sqrt{s} = 8$ TeV. The proton
 336 beam is comprised of bunches of protons with enough spacing that bunch col-
 337 lisions can happen independent of each other. Apart from the energy, the rate at
 338 which the accelerator produces a certain process can be calculated through the
 339 instantaneous luminosity. For the LHC the instantaneous luminosity was 10^{34}
 340 $\text{cm}^{-2}\text{s}^{-1}$ [15] or $10\text{nb}^{-1}\text{s}^{-1}$ where 1 barn(b)= 10^{-24} cm^2 .



341 **Figure 1.6:** Figure showing the LHC and the different detector sites[16].

341 The instantaneous luminosity, often just denoted luminosity, can be defined in
 342 different ways depending on how the collision takes place. For two collinear
 343 intersecting particle beams it is defined as:

$$\mathcal{L} = \frac{f k N_1 N_2}{4\pi \sigma_x \sigma_y} \quad (1.6)$$

344 where N_i are the number of protons in each of the bunches, f is the frequency
 345 at which the bunches collide , k the number of colliding bunches in each beam,
 346 and σ_x (σ_y) is the horizontal (vertical) beam size at the interaction point. Since
 347 the instantaneous luminosity increases quadratically with more protons in each
 348 bunch, increasing the number of protons would be a good strategy to increase
 349 the instantaneous luminosity. However aside from the difficulties to create and
 350 maintain a beam with more particles, a large N_i increases the probability for
 351 multiple collisions per bunch crossing, referred to as pile-up. Pile up will be a
 352 key aspect which is described more in subsection 1.3.5.

353 The expected number of events can be calculated by using the instantaneous lu-
 354 minosity through the following:

$$N = \sigma \int \mathcal{L} dt \equiv \sigma \mathcal{L} \quad (1.7)$$

355 where \mathcal{L} is the integrated luminosity and σ is the cross section which is often
 356 measured in barn. The integrated luminosity is a measurement of total number
 357 of interactions that have occurred over time. Before the LHC was shut down \mathcal{L}
 358 was 20.8 fb^{-1} .

359 The cross section, as explained in subsection 1.2.1, is a measure of the effective
 360 surface area seen by the impinging particles, and as such is expressed in units
 361 of area. The cross section is proportional to the probability that an interaction
 362 will occur. It also provides a measure of the strength of the interaction between
 363 the scattered particle and the scattering center. Further details can be found in
 364 reference [17].

365 1.3.2 ATLAS

366 As seen in figure 1.6, there are several detectors at the LHC. One of these is
 367 ATLAS which is a general purpose detector that uses a toroid magnet. Its goal
 368 is to observe several different production and decay channels. The detector is
 369 composed of three concentric sub-detectors, the Inner detector, the Calorimeters
 370 and the Muon spectrometer [18].

371 The Inner detectors main task is to detect the tracks of the particles. It also mea-
 372 sures the position of the initial proton-proton collision.

373 The Calorimeters, electromagnetic and hadronic, are used to calculate the energy
 374 contained in the different particles. The electromagnetic detects particles which
 375 are charged, and the hadronic those which are neutral.

376 The Muon spectrometer is used to detect signs of muons, which will simply pass
 377 through the other detectors without leaving a trace. It also calculates the energy
 378 and momentum of the muons.

379 The neutrinos escape the ATLAS experiment without being detected, and in this
 380 thesis it is assumed that WIMPS pass through all the detectors without leaving
 381 any trace.

382 1.3.3 Coordinate system

383 The coordinate system of ATLAS, seen in figure 1.7 is a right-handed coordinate
 384 system with the x-axis pointing towards the centre of the LHC ring, and the z-axis
 385 along the tunnel/beam (counter clockwise) seen from above. The y-axis points up-
 386 ward. The origin is defined as the geometric center of the detector. A cylindrical
 387 coordinate system is also used for the transversal plane, (R, ϕ, Z) . For simplicity
 388 the pseudorapidity of particles from the primary vertex is defined as:

$$\eta = -\ln(\tan \frac{\theta}{2}) \quad (1.8)$$

389 where θ is the polar angle (xz-plane) of the particle direction measured from
 390 the positive z-axis. η is through this definition invariant under boosts in the z-
 391 direction.

392 It is quite common to calculate the distance between particles and jets in the
 393 (η, ϕ) space, $d = \sqrt{(\Delta\eta)^2 - (\Delta\phi)^2}$.

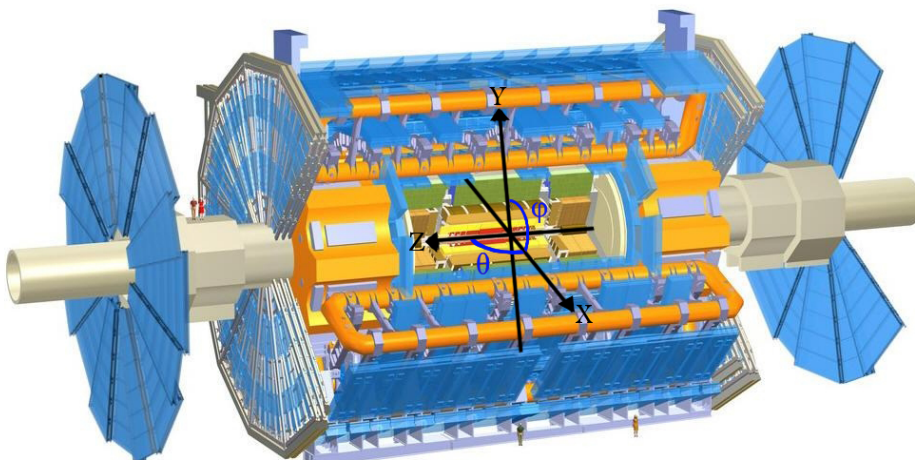


Figure 1.7: The ATLAS detector and the definition of the orthogonal Cartesian coordinate system. Image altered from[19]

394 1.3.4 Reconstructing data

395 To be able to compare the simulated data to real data it is important to include
 396 effects of the detectors. This is done using so called smearing functions which try
 397 to emulate the reconstruction of data.

398 The reconstruction process of data [18] is based on what response is given from
 399 the detectors. It is affected by pile-up and the energy of that which is detected.
 400 This process is not specifically used in the thesis, however the smearing functions
 401 are discussed in section 2.1.

402 1.3.5 Pile-up

403 Pile-up is the phenomena that several proton-proton collisions occur simultaneously.
 404 The number of pile-up is defined as the average number of proton-proton
 405 collisions that occur per bunch crossing per second. It is denoted as $\langle \mu \rangle$. μ can
 406 be calculated by adjusting a Poisson distribution to fit the curve created by the
 407 number of interactions per bunch crossing at a given luminosity. When this is
 408 done μ will be the mean value of the Poisson distribution.

409 1.3.6 Mono-jet analysis

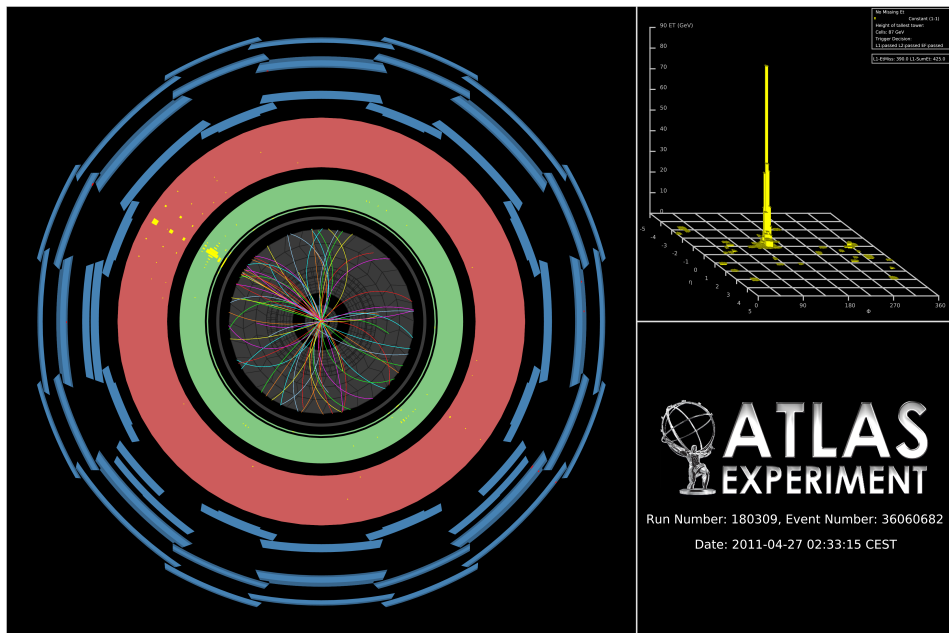


Figure 1.8: Image of an actual mono-jet event recorded by the ATLAS experiment [20].

410 When measuring the transversal energy one can in some interactions find incon-
 411 sistencies, such as jets that are in excess in one direction. In figure 1.8 one can see
 412 a high energetic jet which gives an excess of transversal energy in one direction
 413 after the collision. Since there is no balancing jet there must be transverse energy
 414 that is not detected, denoted E_T^{Miss} , since it was close to zero before the collision.
 415 This gives an indication that there energy to balance this that simply can not be
 416 detected. This could for instance be neutrinos or the sign of a new particle.

417 E_T^{Miss} is the modulus of the E_T^{Miss} vector which is defined as:

$$E_T^{\vec{M}iss} = - \sum E_T^{\vec{jet}} - \sum E_T^{\vec{Electron}} - \sum E_T^{\vec{\mu}on} - \sum E_T^{\vec{T}au} - \sum E_T^{\vec{\gamma}photon} \quad (1.9)$$

418 Jets are hadrons which travel in the same direction and are usually created from

hadronization of a quark or a gluon in a collision. Usually jets are composed of a lot of energetic hadrons.

Since the jets are created from quarks or gluons, measuring a jet results in more information about the collision.

There are two main classes of events, signal and background. The signal corresponds to events that would arise from one of the processes in subsection 1.2.5. However to know that the missing energy is sign of the signal then one must understand all the other components that could contribute to the missing energy. Also there must be an excess of missing energy from what is expected from the background.

The background comprises of standard model processes that can mimic the mono-jet signature.

1.3.7 Phase II high luminosity upgrade

At the moment, the whole LHC is undergoing a step by step upgrade program which will be finalized around 2022-2023, denoted the high luminosity upgrade, or HL-upgrade. The upgrade consists of different stages, meaning that the upgrade will halt for periods so that experiments can take place. In figure 1.9 one can see

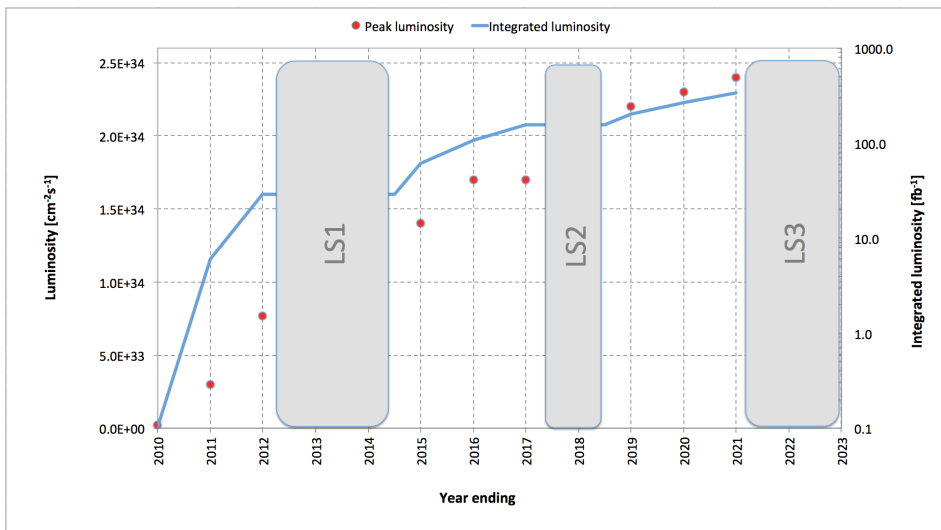


Figure 1.9: A graph showing the upgrading timetable with the instantaneous luminosity, denoted luminosity, and integrated luminosity expected in the different stages.

the three proposed upgrades. The period before LS1 is denoted phase 0, after LS1 and before LS2 phase I and after LS3 phase II.

LS1 is the upgrade which will take the LHC to its designed performance.

- 439 LS2 will take the LHC to the ultimate designed instantaneous luminosity.
 440 LS3 which is the focus of this thesis, will increase the instantaneous luminosity
 441 even more. Though for this to happen a modification of the whole LHC
 442 must be done, instead of just an upgrade and maintenance as before.

443 The following is expected for the experiments done after phase II:

Entity	Expected	Last run (2012)
Instantaneous luminosity	$\mathcal{L} \sim 50 \text{ nb}^{-1} \text{s}^{-1}$	$\mathcal{L} \sim 10 \text{ nb}^{-1} \text{s}^{-1}$
Integrated luminosity	$\mathcal{L} = 1000 - 3000 \text{ fb}^{-1}$	$\mathcal{L} = 20 \text{ fb}^{-1}$
Pile-up	$\langle \mu \rangle = 140$	$\langle \mu \rangle = 20$
Center of mass energy	$\sqrt{s} = 14 \text{ TeV}$	$\sqrt{s} = 8 \text{ TeV}$

Table 1.2: Expected running values for the Phase II HL-upgraded LHC with older values for comparison [21].

444 Where it should be noted that the integrated luminosity indicates the total amount
 445 of data which will be collected after the upgrade is completed before the next up-
 446 grade takes place.

447 1.3.8 Monte Carlo simulation

- 448 As mentioned before, in this thesis only emulated data has been used. This data
 449 is created by using a Monte Carlo (MC) simulation of the background processes
 450 and the expected signal. To do this a program called MadGraph is used.
 451 MadGraph [22] starts with Feynman diagrams and then generates simulated events
 452 based on lots of different parameters.
 453 PYTHIA [23] is a package which adds the correct description of jets to MadGraph
 454 by including hadronization. The correct description of pile-up comes from other
 455 ATLAS software.
 456 The tool to access all this data and analyse it a tool called ROOT, which is used
 457 for programming high energy physics related tools [24].

2

Validation of smearing functions

460 A full detector simulation of the ATLAS detector based on the GEANT [25] pro-
461 gram makes it possible to obtain the expected detector responses to electrons,
462 muons, tau leptons, photons (γ) and jets of hadrons. However these simulations
463 are extremely time-consuming and require a lot of computing power. Also at the
464 present time only a limited set of these simulations exists for the ATLAS phase II
465 upgrade.

466 In this thesis a different strategy is used. Instead of performing a full detector
467 simulation the observed particles from the event generator, which simulates the
468 proton-proton collisions, are smeared by using random numbers following reso-
469 lution functions specific to each type of particle. These emulate how the detector
470 and the reconstruction is affected by the increased luminosity and the pile-up
471 which comes with this.

472 The resolution functions or smearing functions are the official functions devel-
473 oped from previous studies [1, 26] by the ATLAS collaboration for the study of
474 the ATLAS phase II upgrade. The key feature of those studies was that the di-
475 rection of the momenta is unaffected and that only jets and E_T^{Miss} are affected by
476 pile-up. Since this was confirmed in previous studies it was not incorporated into
477 the smearing functions as discussed more in section 2.1.

478 Since part of this thesis work was to take the official ATLAS smearing functions
479 and apply the smearing to each particle, it was important to check that the en-
480 ergy and momenta resolutions of the smeared objects were consistent with the
481 expected values. Thus in this chapter the energy and momenta resolutions are
482 measured after applying the smearing to some simulated processes and the re-
483 sulting resolutions are compared with the expected values.

484 2.1 Smearing functions

485 These smearing functions are designed so that they take into account the effi-
 486 ciency of the different detectors, limitations from how they are constructed as
 487 well as their dependence on pile-up. They also take into account how all this
 488 varies depending on the measured entries energy or momenta.

489 Terminology:

- 490 • Data before smearing, simulated data, is denoted as data at a truth level or
 491 truth data.
- 492 • Data after smearing, which is comparable to what is measured is denoted
 493 as reconstructed or reco data as discussed in subsection 1.3.4.

494 2.1.1 Electron and photon

495 The identification of electrons relies on finding an isolated electron track and
 496 a pattern in the calorimeter compatible with an electron shower. Pile-up will
 497 affect the electrons by decreasing the efficiency to identify an electron because of
 498 the increased number of tracks. However for the identified electrons the energy
 499 resolution will be close to that without pile-up.

500 The electron and photon have the same smearing since they are both detected in
 501 a similar way.

502 2.1.2 Muon

503 The identification of muons relies on isolated tracks in the inner detector being
 504 matched with information in the muon system. Since the muon system is the
 505 outer most detector seen from the collision point it is unaffected by the false
 506 detection effects of pile-up.

507 2.1.3 Tau

508 Tau is detected similarly to electron and photon. In this thesis all tau processes
 509 are assumed to be at 3 prong. Where prong refers to the different amount of
 510 tracks from which they were reconstructed. This in turn means that the effect of
 511 pile-up will be worse compared to an electron as a triplet must be found in an
 512 increased number of tracks.

513 2.1.4 Jets

514 The largest effect of pile-up is to add additional jets in the ATLAS detector. These
 515 additional jets contribute to additional energy deposited inside the existing jets
 516 and to E_T^{Miss} .

517 2.1.5 Missing Transversal Energy

518 E_T^{Miss} , the missing transversal energy, which was discussed in subsection 1.3.6,
 519 and defined in (1.9) is calculated by knowing that there should be energy conser-

vation in the collision. It is comprised of different parts, one from neutrinos, one from errors in the other measurements and one from new physics. It should be affected by pile-up as described above.

2.2 Validation

To validate the smearing functions a comparison with Ref. [26] was made where the standard deviation, depending on the energy or momentum value of an entity, was given, see section 2.4. This is performed using the simulated processes listed in table 2.1.

Table 2.1: Different processes from where data has been taken. Each sample is a simulation of a physical process, the simulation names can be found in appendix A

Particle	Process
Electron	$W \rightarrow e\nu$
Muon	$W \rightarrow \mu\nu$
Tau	$W \rightarrow \tau\nu$
γ	$\gamma + \text{Jet sample}$
Jets	Jet sample
E_T^{Miss}	$Z \rightarrow \nu\nu + \text{Jet sample}$

The energy and momentum resolutions are obtained for each type of particle by comparing the values before and after smearing.

This is done by looking at the reco data for a given slice at a truth energy or momentum value. Since the smearing functions takes a lot into account the match will not be a fine line as seen in figure 2.3b.

By fitting a Gaussian curve to this data will then result in the standard deviation which is used in the validation. The standard deviation is also known as the resolution of the data and will be denoted σ .

This resolution is then compared to previous results, [26].

To get enough statistics enough data must be available for a given truth energy or momenta and the analysis must be specific enough to only look at a narrow enough interval around this point.

Step by step method

- Take a MC sample with a given particle, i.e electrons.
- Choose a slice of electron which have a truth energy of a given value (75 GeV for electrons).
- Plot the smeared electron energy for this slice of truth energy. Given for electrons and photons in figure 2.1.
- For this distribution of smeared energy, fit a Gaussian distribution and calculate the sigma value of this Gaussian.
- Compare this sigma, which is the calculated resolution to the expected resolution given from the smearing functions.

551 2.3 Results

- 552 As discussed above, the method was to plot the data against its smeared counter-
553 part and through this determine σ to see if it conforms to the expected values.
- 554 Only one energy value is shown for simplicity, though the comparison was done
555 for different energy values.
- 556 The average number of pile-up is fixed at 60 as a benchmark unless anything else
557 is stated.
- 558 As the comparison, figure 2.4, figure 2.1, figure 2.2 and figure 2.5 are divided
559 depending on the different η values.
- 560 All results are summarized in table 2.5.

561 2.3.1 Electron and photon

562 Since these interact very similarly in the detector, their smearing functions are
 563 identical. The slice value represents at which value of unsmeared energy or mo-
 564 mentum this smearing occurs.

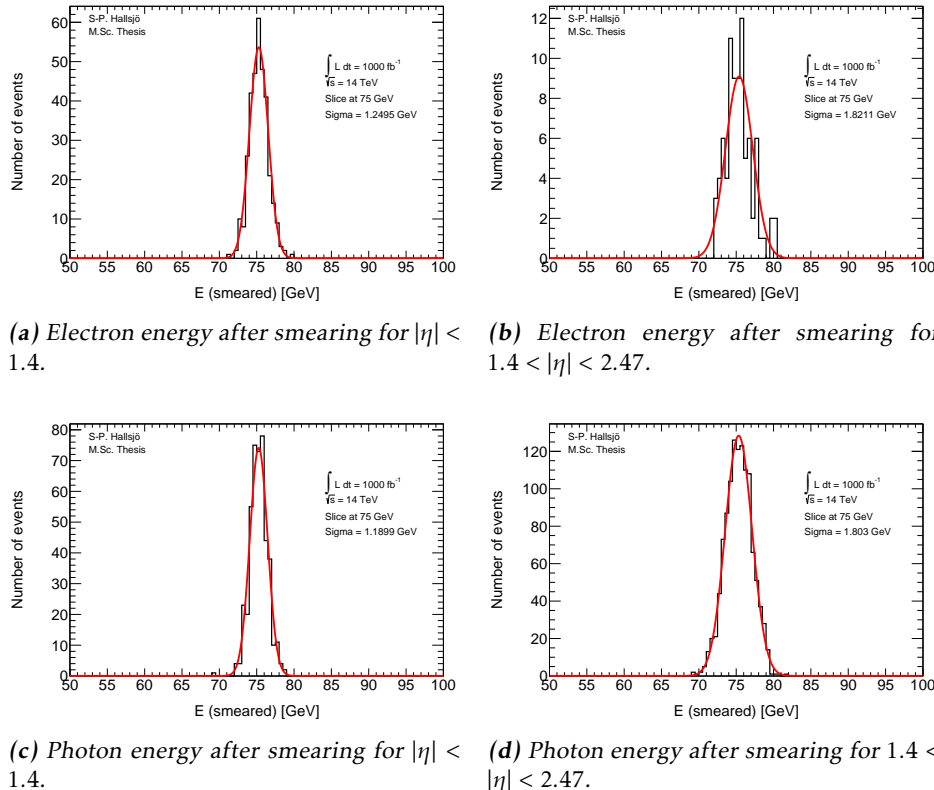
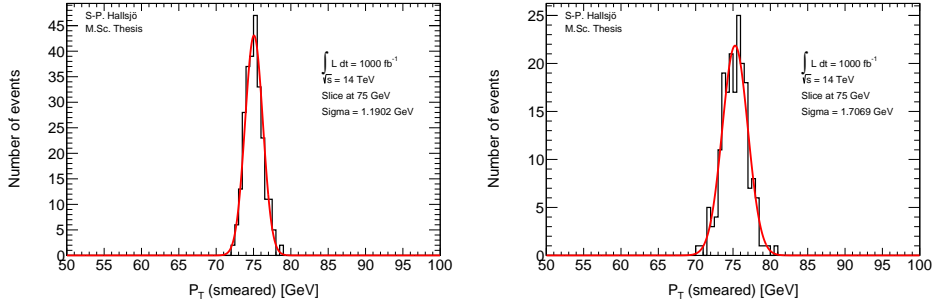


Figure 2.1: Photon and electron energy after smearing.

2.3.2 Muon

Since muons are shielded from the effects of pile-up only efficiency and detector limitations affect the smearing.

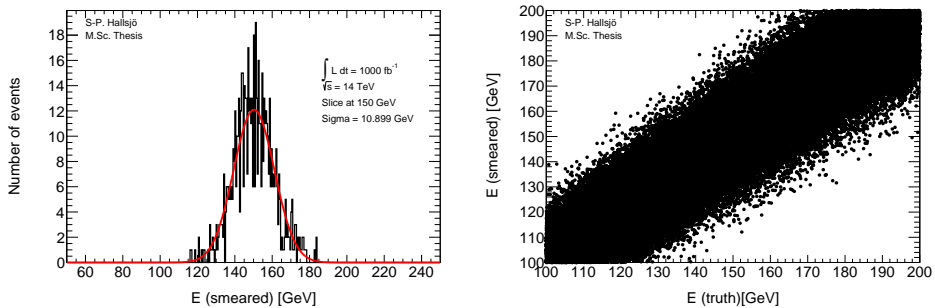


(a) Muon momenta after smearing for $|\eta| < 1.05$. (b) Muon momenta after smearing for $1.05 < |\eta|$.

Figure 2.2: Muon momenta after smearing.

2.3.3 Tau

As described in subsection 2.1.3 tauons are detected similarly to electrons and photons. Thus the plots should look similarly to those in the previous subsection apart from the slice being at 150 GeV. In figure 2.3a the Gaussian fit (red) and the data (black) are given for tau detected through 3 prong. In figure 2.3b smeared versus truth energy is shown.



(a) Tau energy after smearing.

(b) Tau energy vs smeared.

Figure 2.3: Tau energy after smearing and energy vs smearing.

2.3.4 Jets

Jets as described in subsection 1.3.6, are hadronic showers. The smearing functions are divided into four different regions depending on the angle η .

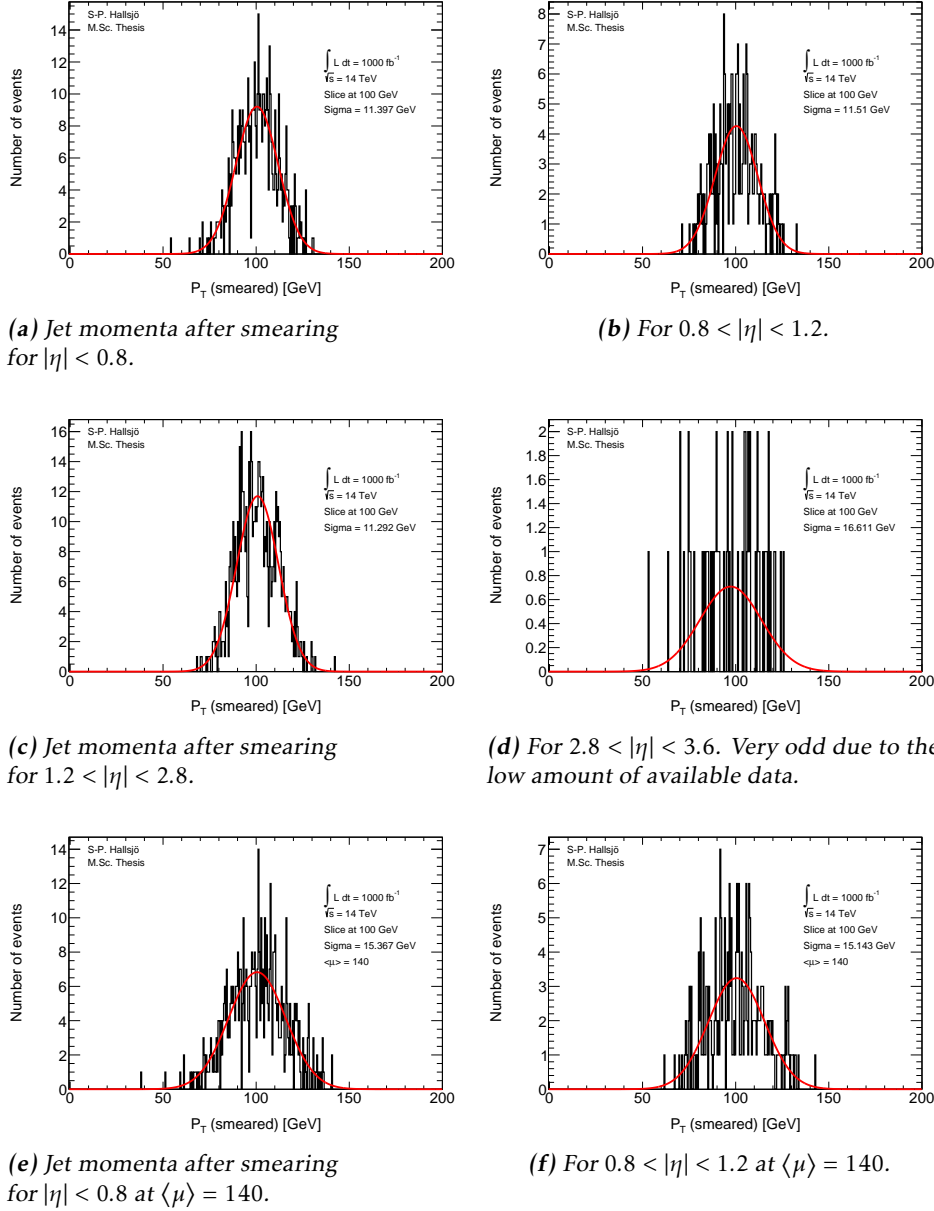


Figure 2.4: Jet momenta after smearing.

577 2.3.5 Missing Transversal Energy

578 The figures in this subsection are, compared to the above, given as absolute smear-
 579 ing, thus at 0 it represents that the energy is unsmeared, compared to the others
 580 where the slice value represents the unsmeared.

581 Here the E_T^{Miss} is projected down to the x- and y-axis, since these are the transver-
 582 sal axes, to be smeared.

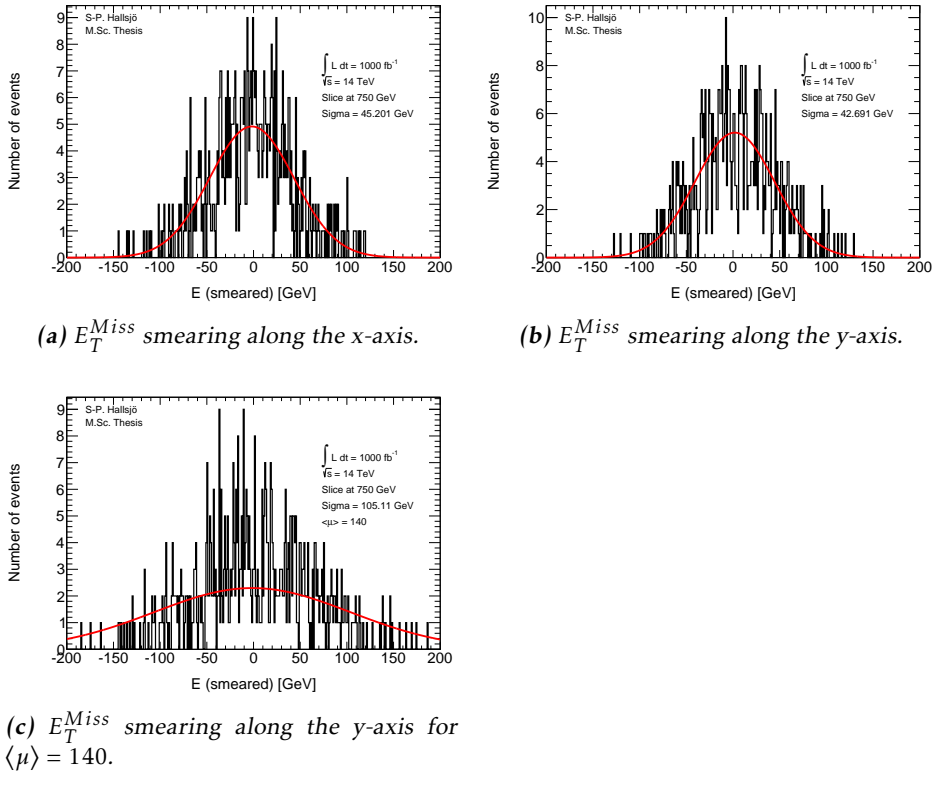


Figure 2.5: E_T^{Miss} smearing plots

2.4 Expected results

583 Since the leptons and photons are all detected by fitting detectors responses to
 585 different tracks, meaning that the effect of pile-up should be that there are more
 586 track to match, but it should not affect which ones are matched. The indepen-
 587 dence of pile-up for leptons and photons is backed up in previous research, for
 588 instance [1, 27].

589 To validate the smearing code, comparisons were made with [26] which gave the
 590 following formulation for the expected σ :

Observable	Absolute σ
Electron & photon	$\sigma = 0.3 \oplus 0.1\sqrt{E(GeV)} \oplus 0.01E(GeV), \eta < 1.4$ $\sigma = 0.3 \oplus 0.15\sqrt{E(GeV)} \oplus 0.015E(GeV), 1.4 < \eta < 2.47$
Muon momentum	$\sigma = \frac{\sigma_{id}\sigma_{ms}}{\sigma_{id} \oplus \sigma_{ms}}$ $\sigma_{id} = P_T(a_1 \oplus a_2 P_T)$ $\sigma_{ms} = P_T(\frac{b_0}{P_T} \oplus b_1 \oplus b_2 P_T)$
Tau energy	$\sigma = (0.03 \oplus \frac{0.76}{\sqrt{E(GeV)}})E(GeV)$, for 3 prong.
Jet momentum	$\sigma = P_T(GeV)(\frac{N}{P_T} \oplus \frac{S}{\sqrt{P_T}} \oplus C)$ where $N = a(\eta) + b(\eta)\mu$
E_T^{Miss}	$\sigma = (0.4 + 0.09\sqrt{\mu})\sqrt{\sum E(GeV) + 20\mu}$

Table 2.2: Expected absolute σ where the parameters are given for muons in table 2.3 and for jets in table 2.4. Functions take from [26].

	a_1	a_2	b_0	b_1	b_2
$ \eta < 1.05$	0.01607	0.000307	0.24	0.02676	0.00012
$ \eta > 1.05$	0.03000	0.000387	0.00	0.03880	0.00016

Table 2.3: Parameters used in the muon smearing function taken from [26].

$ \eta $	a	b	s	C
0-0.8	3.2	0.07	0.74	0.05
0.8-1.2	3.0	0.07	0.81	0.05
1.2-2.8	3.3	0.08	0.54	0.05
2.8-3.6	2.8	0.11	0.83	0.05

Table 2.4: Parameters used in the jet smearing function taken from [26].

Process	σ [GeV]	Expected σ
Electron low η	1.25 ± 0.05	1.18
High η	1.82 ± 0.14	1.74
Photon low η	1.19 ± 0.04	1.18
High η	1.80 ± 0.04	1.74
Muon low η	1.19 ± 0.05	1.50
High η	1.71 ± 0.09	2.18
Tau	10.90 ± 0.31	10.34
Jet low η	11.40 ± 0.35	11.60
$\langle \mu \rangle = 140$	15.37 ± 0.47	15.77
Mid low η	11.51 ± 0.52	11.94
$\langle \mu \rangle = 140$	15.14 ± 0.68	15.95
Mid high η	11.29 ± 0.31	10.94
High η	16.61 ± 1.53	13.50
E_T^{Miss} x-axis	45.20 ± 1.35	48.45
E_T^{Miss} y-axis	42.69 ± 2.28	48.45
$\langle \mu \rangle = 140$	105.11 ± 12.24	87.28

Table 2.5: σ values.

- Where the given σ is still the absolute.
- Where the large difference between calculated and expected σ for Muons and E_T^{Miss} is explained by incorrectly calculated errors in σ .

591

592

593

594 2.5 Discussion

595 2.5.1 Smearing independent on pile-up

596 From the validation done it was interesting to note that the smearing functions
597 were created from previous studies, [1, 27], which had shown that leptons and
598 photons are not affected by pile-up. This may seem incredible however it be-
599 comes quite logical when one understands how the detectors work. To be able to
600 detect particles the detectors must detect an excess of energy which comes from
601 a particle passing through. This should not be distorted by an increased pile-up.
602 The amount of particles passing through will of course increase, but the detec-
603 tions should be unaffected as well as the recreation of the events. However with
604 the same logic it makes sense that jets and E_T^{Miss} are quite affected since they
605 are combined of several parts, either hadronic particles or by all the transversal
606 missing energy.

607 Another interesting part is how the effect diminishes with and increasing energy.
608 As seen above, and through the the formula, for the high energies which were of
609 interest here the effect is minimal.

610 2.5.2 Comparison to expected results

611 One of the major problems in the comparison was to get the significance of the
612 Gaussian fit to be calculated correctly. The tool ROOT has a lot of different fea-
613 tures which made this task somewhat difficult. Also since this is a statistical
614 property there is a statistical fluctuation in the result.

615 Another was to retrieve the correct values from the paper, [26], since it was un-
616 clear if the values given were absolute or scale dependent. This has now been
617 corrected in a new version of the paper.

618 **2.6 Conclusion**

- 619 The smearing functions work as intended within 5.8 sigma, however when using
620 a test box and averaging the sigmas one ends up with half of this for the extreme
621 cases, muons and E_T^{Miss} y-axis.

3

Evaluating dark matter signals

624 **Disclaimer: All data provided is still a work in progress and may be subject to
625 change before the final version.**

626 The main goal of the thesis is to investigate if certain dark matter signals can
627 be detected after the high luminosity upgrade. One immediate worry is that the
628 background will be large in comparison to the signal, making the signal undetectable.

630 Another goal is to investigate if it might become more difficult to differentiate
631 between the signal and background due to the degradation of jet and missing
632 energy resolutions in the high luminosity upgrade.

633 This thesis focus on using a luminosity at 1000 fb^{-1} and a center of mass energy
634 at 14 TeV. The reco data is created using a pile-up rate, $\langle \mu \rangle = 140$ as expected
635 during phase II.

636 The signal models are given in appendix A along with the background models.
637 The different models were introduced subsection 1.2.5 and will be discussed in
638 more detail in this chapter.

639 Each signal model has been evaluated in different signal regions and the de-
640 tectability has been evaluated using a statistical P-value. This process has been
641 performed at a pile-up value of 140, as expected for after the high luminosity
642 upgrade.

643 3.1 Signal to background ratio

644 3.1.1 Signal Region

645 A signal region (SR) is defined as a set of selections on event variables designed
 646 to create a sample which is enriched in signal and depleted of background. One
 647 usually tries to design the signal region so that the signal is large enough and the
 648 background small enough that one would statistically be able to either:

- 649 • Exclude the signal if the observation of the data is compatible with a back-
 650 ground only hypothesis.
- 651 • Detect the signal and quantify the significance of the excess in data over
 652 background if the data is consistent with a signal + background hypothesis.

653 An event is a recorded proton-proton collision which consists of hundreds or
 654 thousands of observables such as the number of electrons, muons, jets, tau leptons,
 655 gammas or E_T^{Miss} each with their energy and momenta.

656 To define an optimal signal region is not known a priori and has to be studied for
 657 different signal models. The optimal region typically changes e.g with a change
 658 of the mass of new particles for instance the WIMP mass or the suppression scale.
 659 This is why there are several different signal regions to be studied in this thesis.

660 3.1.2 Weight

661 A weight is used to normalize different types of data so that they can be compared.
 662 As given in (1.7), the total number of events can be estimated as:

$$N = \sigma \int \mathcal{L} dt \equiv \sigma \mathcal{L} \quad (3.1)$$

663 Thus, if all events are generated at different luminosities, depending on the com-
 664 puting power of the computer which performed the simulation, the following
 665 weight should be used to receive the events at a new luminosity:

$$weight = \frac{\mathcal{L}\sigma}{N_{Raw}} \quad (3.2)$$

666 where N_{Raw} is the number of events expected at the luminosity that was set to cre-
 667 ate the data, compared to \mathcal{L} which is the luminosity at which the data is compared
 668 and σ is the cross-section. In this thesis the luminosity is fixed at $\mathcal{L} = 1000\text{fb}^{-1}$.

669 3.1.3 Verification of background normalization

670 To verify that the background samples are correctly normalized they are com-
 671 pared with Ref. [28] in which the center of mass energy is 8 TeV and the lumi-
 672 nosity is 10 fb^{-1} . Since the luminosity is not 1000 fb^{-1} as used in this thesis the
 673 expected values from the paper scaled up with a factor 100 to be comparable.

674 Somewhat unexpectedly a center of mass energy at 8 TeV had cross-sections a fac-
 675 tor 4 lower than the cross-sections at 14 TeV. These cross-sections are generated

either with MadGraph[22] or PYTHIA[23] depending on the generator given for each dataset in appendix A.

The signal regions used in the article were the following:

Selection Criteria		
Jet veto, require no more than 2 jets with $p_T > 30\text{GeV}$ and $ \eta < 4.5$		
Lepton veto, no electron or muon		
Leading jet with $ \eta < 2.0$ and $\Delta\phi(\text{jet}, E_T^{Miss}) > 0.5$ (second-leading jet)		
signal region	SR3p	SR4p
minimum leading jet p_T (GeV)	350	500
minimum E_T^{Miss} (GeV)	350	500

Table 3.1: The signal regions from Ref. [28].

The article [28] has in total four signal regions, unfortunately since the simulated events used in this thesis are filtered before the analysis only the two highest regions are comparable. This can be seen in table 3.3 in subsection 3.4.1.

3.1.4 Errors in data

To make a thorough analysis of the background it is important to take into consideration different errors that exist in the number of events. This is especially important when looking at which signals can be excluded in different signal regions. There exists three main types of errors:

- Statistical errors from MC.
- Statistical errors from the control region.
- Systematic errors.

The statistical errors from MC come from the method of generating background events and is unfortunately nothing that can be estimated when one is not generating the events.

The statistical errors from the control region require an explanation of what a control region is. A control region (CR) is similar to a signal region, a set of criteria which are imposed on the data. This criteria are not set so that there can be a region with almost no signal. In this CR there will still be fluctuations in the amount of background events due to statistical effects, which can then be measured.

The systematic errors is a fixed error which is always present coming from different approximations in how all the events were generated.

3.1.5 Figure of merit

To be able to evaluate different signal regions and different signal models, a figure of merit p is used. The value p is the probability for the background to fluctuate

to the value of the signal + background. Thus if the p-value is small, regardless if the signal is large or the background or its fluctuations are small, it is improbable that the background could result in the same value as if there was a signal and background. This means that for a sufficiently small p-value the signal is detectable.

Assuming the expected number of background events are $B \pm \sigma_B$ where σ_B is the quadratic sum of the statistical error from Monte Carlo, the statistical error from the control region (CR) and the systematic errors as explained in subsection 3.1.5. The expected number of signal events is S , assumed without fluctuation.

If no uncertainty in B or S is assumed, then the probability that the background will fluctuate up to the signal and background should follow a Poisson distribution as such:

$$P(S+B|B) = \frac{e^{-B} B^{(S+B)}}{(S+B)!} \quad (3.3)$$

The probability that the background will fluctuate to a value N larger or equal to the signal and background then becomes:

$$P(B \geq S+B|B) \equiv P(N|B) = \sum_{N=S+B}^{\infty} \frac{e^{-B} B^N}{N!} \quad (3.4)$$

However since there is an uncertainty in the background, the probability distribution $P(N|B)$ must be convoluted with a Gaussian function:

$$G(N_B|B, \sigma_B) = \frac{1}{\sigma_B \sqrt{2\pi}} e^{-\frac{(N_B-B)^2}{2\sigma_B^2}} \quad (3.5)$$

where N_B is the expected number of background events. The convolution is done using N_B as B resulting in the total probability density function:

$$\begin{aligned} F(N|N_B, \sigma_B) &= P(N|B)*G(N_B|B, \sigma_B) = \\ &= \int_{-\infty}^{\infty} P(N|N_B - B) G(N_B|B, \sigma_B) dN_B \end{aligned} \quad (3.6)$$

Inserting the sum over N leads to the probability of the background fluctuation to signal and background being obtained as.

$$p = \sum_{N=S+B}^{\infty} \int_{-\infty}^{\infty} P(N|N_B - B) G(N_B|B, \sigma_B) dN_B \quad (3.7)$$

In this thesis, two different models of the error in the background σ_B are used. Both models are based on Ref. [28]. As described in the beginning of this subsection the error is calculated as:

$$\sigma_B = \text{Statistical error from MC} \oplus \text{Statistical error in CR} \oplus \text{Systematic error}$$

- The statistical error from MC has been neglected since there is no way of estimating it.
- The statistical error from background CR has been taken from the article and assumed to decrease with the increased luminosity as, $\frac{30}{380} \frac{\sqrt{L_{old}}}{\sqrt{L_{new}}}$
- The systematic error has been given two different values, from the article: $\frac{30}{380}$ or fixed at 0.02.
- All this results the total error being used as either, 0.08 or 0.02.

3.1.6 D5 operator models

As described in subsection 1.2.5, one of the signals is modelled using the D5 operator. In this thesis two different scenarios are used, one at a dark matter mass of 50 GeV and one at 400 GeV.

Each of these models are modelled with a mass suppression scale, denoted M^* , which is connected to the cross-section of the process through:

$$\sigma_{new} = \frac{\sigma_{old}}{M^*} \quad (3.8)$$

In subsection 3.4.3 it is determined which values of M^* could be excluded with the upgraded LHC phase 2 upgrade and ATLAS.

3.1.7 Light vector mediator models

As described in subsection 1.2.5, the other signal model is a vector mediator model. In this thesis these signals have two different width scenarios and a number of different mediator mass scenarios. **Where width is related to the lifetime of the dark matter particle.** In addition to this there are, as with the D5 operator, two different dark matter masses, one at 50 GeV and one at 400 GeV.

The result of the investigation of which models are excludable with the upgraded LHC phase 2 upgrade and ATLAS are given in subsection 3.4.6.

3.2 Signal region definitions

3.2.1 Signal regions

To be able to compare signal results to previous papers new signal regions were devised. It was also discovered that the requirement of no electrons was to harsh for the signal models. Because of this new signal criteria were devised.

Selection Criteria

Jet veto, require no more than 2 jets with $p_T > 30\text{GeV}$ and $|\eta| < 4.5$

Lepton veto, no electron or muon.

The electron veto is defined: $\Delta R(jet^{lead}, electron^{lead}) \geq 0.4$ and $electron^{lead} p_T > 20\text{GeV}$ removed.

Leading jet with $|\eta| < 2.0$ and $\Delta\phi(jet, E_T^{Miss}) > 0.5$ (second-leading jet)

signal region	SR1	SR1p	SR2	SR3	SR4
minimum leading jet p_T (GeV)	350	500	600	800	1000
minimum E_T^{Miss} (GeV)	350	500	600	800	1000
signal region	SRa	SRb	SRc	SRd	
minimum leading jet p_T (GeV)	350	350	350	350	
minimum E_T^{Miss} (GeV)	350	600	800	1000	

Table 3.2: The new signal regions

3.2.2 Verifying background data

To make sure that the altered electron veto still produces results comparable with [28] a comparison is made again. This can be seen in subsection 3.4.1 in table 3.4.

3.3 Mitigating the effect of the high luminosity

As discussed in subsection 2.5.1 the smearing functions effect of pile-up should be minimal in the high energy regions which are of interest in this thesis.

From the formulation of the smearing functions, the biggest effect should be seen at low energies. This is related to the difficulty for the hardware triggers to select events. This means that one drawback of the high luminosity upgrade is that very low energy signal regions will be lost.

The effect of the high luminosity is seen in the results in subsection 3.4.4, subsection 3.4.7 and discussed in subsection 3.5.2

762 3.4 Results

763 3.4.1 Verifying background data

764 In table 3.3 and table 3.4 a comparison has been made between the number of
 765 simulated background events at a truth level and the number of expected events
 766 by scaling up the values from Ref. [28] by a factor 100. Truth data was used to
 767 not let the increased pile-up value affect the comparison. It can be seen that the
 768 simulated events and expected events coincide quite well on all accounts apart
 769 from $W \rightarrow \tau\nu$, $W \rightarrow \mu\nu$ and thus the total as well.

770 The difference in $W \rightarrow \tau\nu$ can be explained by the fact that τ can not be recreated
 771 as a jet in the simulated events which it can in measured events.

772 The difference in $W \rightarrow \mu\nu$ is explained through the simulated events having a
 773 better separation of muons neutrinos and E_T^{Miss} .

Process	SR3p	Expected SR3p	SR4p	Expected SR4p
$Z \rightarrow \nu\nu$	140298	152000	25250	27000
$W \rightarrow \tau\nu$	40701	37000	5862	3900
$W \rightarrow e\nu$	11229	11200	1507	1600
$W \rightarrow \mu\nu$	13727	15800	1872	4200
Total background	205955	218000	34491	36700

Table 3.3: Comparison of the simulated and expected events from Ref. [28] with $\mathcal{L} = 1000\text{fb}^{-1}$, cross-sections corresponding to $\sqrt{s} = 8\text{TeV}$ and using the same electron veto.

Process	SR1	Expected SR1	SR1p	Expected SR1p
$Z \rightarrow \nu\nu$	147009	152000	26734	27000
$W \rightarrow \tau\nu$	44728	37000	6544	3900
$W \rightarrow e\nu$	17964	11200	2470	1600
$W \rightarrow \mu\nu$	14286	15800	1972	4200
Total background	223986	218000	37720	36700

Table 3.4: Comparison of the simulated and expected events from Ref. [28] with $\mathcal{L} = 1000\text{fb}^{-1}$, cross-sections corresponding to $\sqrt{s} = 8\text{TeV}$ and using a modified electron veto.

774 3.4.2 Events

775 In the following tables the number of events are given using one of the D5 opera-
 776 tors as the signal, and the background in the different signal regions. The number
 777 of background events is also used for the vector mediator signals.

Process	SR1	SR2	SR3	SR4	SRa	Srb	Src	Srd
D5, mDm=50 GeV, M*=1TeV	129863	30219	10750	4391	129863	36410	12927	5221
Z $\rightarrow \nu\nu$	604479	42657	8424	2111	604479	58614	11383	2843
W $\rightarrow \tau\nu$	154140	7807	1308	295	154140	10679	1788	386
W $\rightarrow e\nu$	61772	2890	485	110	61772	3961	654	152
W $\rightarrow \mu\nu$	49114	2357	379	91	49114	3052	499	108
Total background	869505	55711	10597	2607	869505	76305	14325	3489

Table 3.5: Signal and background events for truth data in the signal regions.

Process	SR1	SR2	SR3	SR4	SRa	Srb	SRc	SRd
D5, mDm=50 Gev, M*=1TeV	120295	28019	9978	4130	120295	38762	13752	5505
Z $\rightarrow \nu\nu$	553735	39105	7681	1932	553735	71613	13145	3140
W $\rightarrow \tau\nu$	156023	7741	1282	276	156023	14500	2174	467
W $\rightarrow e\nu$	58874	2706	448	106	58874	5177	790	176
W $\rightarrow \mu\nu$	47801	2299	380	89	47801	4031	618	139
Total background	816433	51850	9791	2404	816433	95322	16727	3922

Table 3.6: Signal and background events for reco data with $\langle\mu\rangle = 140$ in the signal regions.

778 **Disclaimer: The thesis is not completed after here.**

779 3.4.3 Limit on M^*

780 For the D5 operators as described in subsection 3.1.6 the mass suppression has
 781 been calculated by evaluating at which point the signal is covered by the back-
 782 ground. This is done using the two different error models as described in subsec-
 783 tion 3.1.5 as figures of merit.

784 The limit is found, seen as a horizontal line, when the p-value = 0.05.

785 Give at 1000fb-1 and with 14 TeV cross-sections. And for the different signal
 786 regions. Refer to M^* explained in subsection d5. subsection 3.1.6

787 Simply figures for one signal and error model. Otherwise it would take alot of
 788 space.

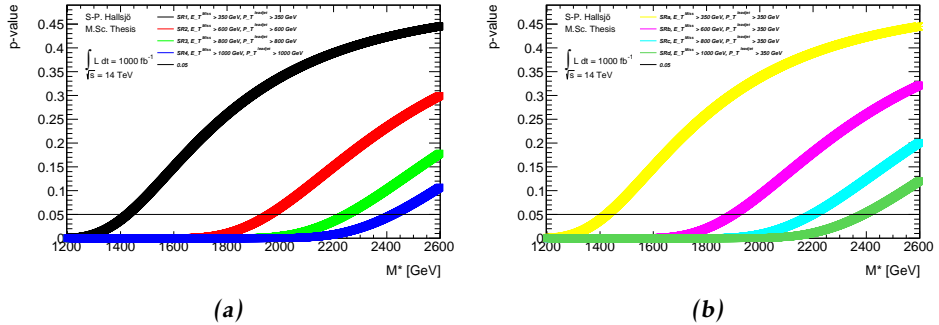


Figure 3.1: On a truth level error model 0.02.

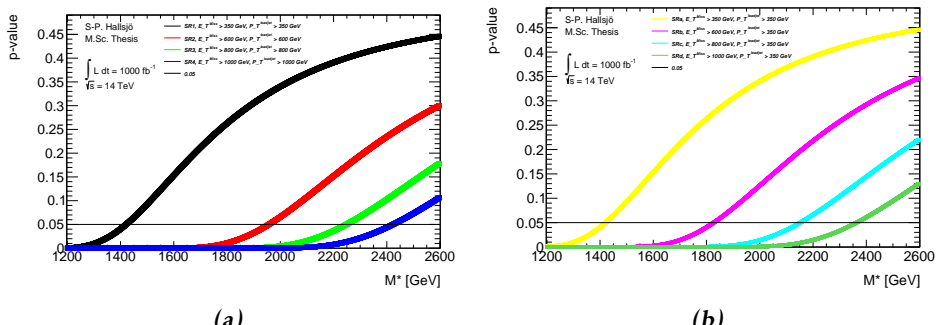


Figure 3.2: On a reco level error model 0.02.

Signal region	M* Truth data [GeV]	Reco data [GeV]
SR1	1425	1420
SR2	1960	1957
SR3	2249	2248
SR4	2423	2423
SRa	1425	1421
SRb	1900	1827
SRc	2197	2152
SRd	2389	2363

Table 3.7: Mass suppression scales in GeV given for $mDm=50$ and the 0.02 error model.

Signal region	M* Truth data [GeV]	Reco data [GeV]
SR1	1015	1012
SR2	1400	1400
SR3	1636	1637
SR4	1846	1854
SRa	1015	1012
SRb	1356	1303
SRc	1589	1553
SRd	1796	1768

Table 3.8: Mass suppression scales in GeV given for $mDm=50$ and the 0.08 error model.

789 3.4.4 Effect of pile-up on M^*

790 As seen in the data above, refer to tables, how big is the effect maximum? Since
 791 no error bars are given, perhaps no concrete results.

792 Seems to be a minimal effect atleast.

793 3.4.5 Previous results

794 10fb paper. Preliminary not that much better results for 1000fb-1 and 14TeV.

795 The whole discussion with Steven and David.

796 3.4.6 Limit on mediator mass

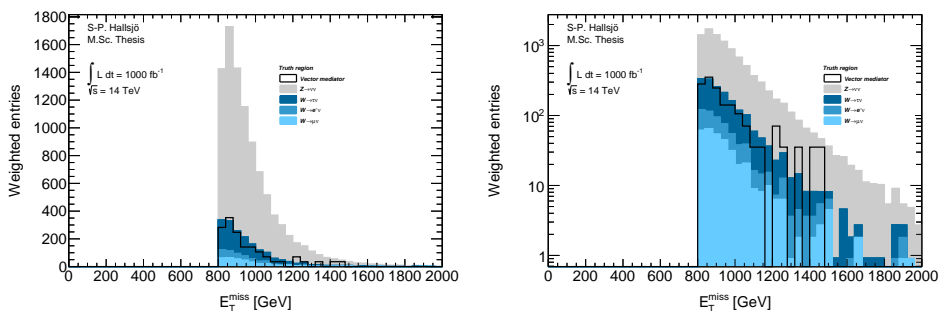
797 Are there previous results? Signal vs background plot in normal and log scale for
 798 one of the vector mediator models, to be able to evaluate all the different models
 799 the so called p-value was used in different signal regions. Below are two figures
 800 showing one of the vector mediator models in SR3p.

Signal region	M* Truth data [GeV]	Reco data [GeV]
SR1	7780	7832
SR2	8350	8280
SR3	8360	8400
SR4	8000	7900
SRa	7780	7832
SRb	8185	8080
SRc	8310	8270
SRd	8060	8030

Table 3.9: Mass suppression scales in GeV given for $mDm=400$ and the 0.02 error model.

Signal region	M* Truth data [GeV]	Reco data [GeV]
SR1	5550	5580
SR2	5965	5920
SR3	6080	6120
SR4	6100	6040
SRa	5550	5580
SRb	5850	5770
SRc	6010	5970
SRd	6060	6000

Table 3.10: Mass suppression scales in GeV given for $mDm=400$ and the 0.08 error model.



(a) Signal on background plot for E_T^{miss} on reco level in SR3.

(b) The same as a) with log scale on the y-axis

Figure 3.3: Signal on background plot to illustrate the a general plot. (OLD)

801 To set a limit on the mediator mass the p-value is calculated in different signal re-
 802 gions for the different signal models with different mediator mass. This resulted
 803 in the following plot.

804 The limit is found when the p-value = 0.05.

805 A table will be given with those models which survived in SR2 and SR3, truth
806 and reco. Should SR4 be there?

807 **3.4.7 Effect of pile-up on mediator mass**

808 What is surprising is that if any model is viable in either truth or reco scenario
809 with any of the error-models, then it is viable for the rest.

810 Check the different cases for reco and truth to see what happens.

3.5 Discussion**3.5.1 Comparison to previous results****3.5.2 Effect of the high luminosity**

Even though this was envisioned as the primary focus of the thesis, it is shown that the effect of pile-up is minute for these high signal regions. Thus the focus was shifted to perform a more in-depth mono-jet analysis of different DM signal models.

Or is the effect high? Work in progress.

819 **3.6 Conclusion**

820 **3.6.1 Limit on M^***

821 **3.6.2 Limit on mediator mass**

822

4

823

Results and Conclusions

824 **Disclaimer: This chapter is not yet complete.**

825 4.1 Validation of smearing functions

826 Have some discussion.

827 Result they appear to work as expected, the reference paper was a bit unclear, I
828 leave my writing as a better reference.

829 **4.2 Signal to background ratio**

830 **4.2.1 Limit on M***

831 **4.2.2 Limit on mediator mass**

832 **4.3 Other selection criteria and observables**

833 **4.3.1 Limit on M***

834 **4.3.2 Limit on mediator mass**

835 **4.4 Mitigating the effect of the high luminosity**

836 **4.5 Recommendations to mitigate the effect of the 837 high luminosity**

838 Keep to a higher energy region, or signal region.

839 **4.6 Suggestions for future research**

840 With more time, search for new signal regions, the only solution now for the HL
841 is to go up in energy. Since none of the other parameters (eta,phi etc) seem to be
842 altered these can not be used. Is there something that has been overlooked?

843 Test the effect of pile-up for lower signal regions? See if the effect is as great as
844 predicted.

845 Explore other theoretical models for dark matter, other d operators etc. Models
846 that are based on Supersymmetry and not just effective theories.

847 Sätt av ett kort kapitel sist i rapporten till att avrunda och föreslå räkningar för
848 framtida utveckling av arbetet.

849 Saving as reference. test citing as: Here we cite Duck [29] [29].

850 If the above works, remember to edit myreferences.

Appendix

852

A

853

Datasets

854 **Disclaimer:** This appendix is not yet complete.

855 A.1 Background processes

856 All datasets used are d4pd.

857 A.1.1 Validation

858 For the validation the following datasets were used, with a filter at generator level
859 at 450GeV for lead jet and MET.

860 mc12 157539 sherpa ct10 znunupt280 v03 mc12 157534 sherpa ct10 wenupt200
861 v03

862 mc12 157535 sherpa ct10 wmunupt200 v03

863 mc12 157536 sherpa ct10 wtaunupt200 v03

864 mc12 129160 pythia8 au2cteq6l1 perf jf17 v03

865 mc12 129160 pythia8 au2cteq6l1 perf jf17 v04

866 mc12 129170 pythia8 au2cteq6l1 gammajet dp17 v04

867 They should be read as such: Monte Carlo version, dataset number, generator, ?
868 name.

869 A.1.2 Background to signals

870 The same as the above though now with the filter as indicated by their name. The
871 second znunu sample has been generated with and center of mass energy at 8
872 TeV.

873 mc12 157539 sherpa ct10 znunupt280 v05

```

874 mc12 157539 8tev sherpa ct10 znunupt280 v05
875 mc12 157536 sherpa ct10 wtaunupt200 v05
876 mc12 157534 sherpa ct10 wenupt200 v05
877 mc12 157535 sherpa ct10 wmunupt200 v05

```

878 A.2 Signals

879 A.2.1 Qcut

880 Qcut means that the original data has been split into different parts depending
 881 on the value of the lead jet pt.

882 A.2.2 D5 signal processes

```

883 mc12 188408 madgraphpythia auet2bcteq6l1 d5 dm50 ms10000 qcut200 v06
884 mc12 188409 madgraphpythia auet2bcteq6l1 d5 dm50 ms10000 qcut400 v06
885 mc12 188410 madgraphpythia auet2bcteq6l1 d5 dm50 ms10000 qcut600 v06
886 mc12 188411 madgraphpythia auet2bcteq6l1 d5 dm400 ms10000 qcut200 v06
887 mc12 188412 madgraphpythia auet2bcteq6l1 d5 dm400 ms10000 qcut400 v06
888 mc12 188413 madgraphpythia auet2bcteq6l1 d5 dm400 ms10000 qcut600 v06

```

889 **All signals should be read as such: Monte Carlo version, dataset number, generator, ?, name of operator, dark matter mass, default mass suppression scale, qcut part.** As discussed in reference

892 A.2.3 Light vector mediator processes

```

893 mc12 188414 madgraphpythia auet2bcteq6l1 dmv dm50 mm100 w3 qcut200
894 v06
895 mc12 188422 madgraphpythia auet2bcteq6l1 dmv dm50 mm100 w3 qcut400
896 v06
897 mc12 188430 madgraphpythia auet2bcteq6l1 dmv dm50 mm100 w3 qcut600
898 v06
899 mc12 188415 madgraphpythia auet2bcteq6l1 dmv dm50 mm300 w3 qcut200
900 v06
901 mc12 188423 madgraphpythia auet2bcteq6l1 dmv dm50 mm300 w3 qcut400
902 v06
903 mc12 188431 madgraphpythia auet2bcteq6l1 dmv dm50 mm300 w3 qcut600
904 v06
905 mc12 188416 madgraphpythia auet2bcteq6l1 dmv dm50 mm500 w3 qcut200
906 v06
907 mc12 188424 madgraphpythia auet2bcteq6l1 dmv dm50 mm500 w3 qcut400
908 v06
909 mc12 188432 madgraphpythia auet2bcteq6l1 dmv dm50 mm500 w3 qcut600
910 v06

```

```
911 mc12 188417 madgraphpythia auet2bcteq6l1 dmv dm50 mm1000 w3 qcut200
912 v06
913 mc12 188425 madgraphpythia auet2bcteq6l1 dmv dm50 mm1000 w3 qcut400
914 v06
915 mc12 188433 madgraphpythia auet2bcteq6l1 dmv dm50 mm1000 w3 qcut600
916 v06
917 mc12 188418 madgraphpythia auet2bcteq6l1 dmv dm50 mm3000 w3 qcut200
918 v06
919 mc12 188426 madgraphpythia auet2bcteq6l1 dmv dm50 mm3000 w3 qcut400
920 v06
921 mc12 188434 madgraphpythia auet2bcteq6l1 dmv dm50 mm3000 w3 qcut600
922 v06
923 mc12 188419 madgraphpythia auet2bcteq6l1 dmv dm50 mm6000 w3 qcut200
924 v06
925 mc12 188427 madgraphpythia auet2bcteq6l1 dmv dm50 mm6000 w3 qcut400
926 v06
927 mc12 188435 madgraphpythia auet2bcteq6l1 dmv dm50 mm6000 w3 qcut600
928 v06
929 mc12 188420 madgraphpythia auet2bcteq6l1 dmv dm50 mm10000 w3 qcut200
930 v06
931 mc12 188428 madgraphpythia auet2bcteq6l1 dmv dm50 mm10000 w3 qcut400
932 v06
933 mc12 188436 madgraphpythia auet2bcteq6l1 dmv dm50 mm10000 w3 qcut600
934 v06
935 mc12 188421 madgraphpythia auet2bcteq6l1 dmv dm50 mm15000 w3 qcut200
936 v06
937 mc12 188429 madgraphpythia auet2bcteq6l1 dmv dm50 mm15000 w3 qcut400
938 v06
939 mc12 188437 madgraphpythia auet2bcteq6l1 dmv dm50 mm15000 w3 qcut600
940 v06
941 mc12 188438 madgraphpythia auet2bcteq6l1 dmv dm50 mm100 w8pi qcut200
942 v06
943 mc12 188446 madgraphpythia auet2bcteq6l1 dmv dm50 mm100 w8pi qcut400
944 v06
945 mc12 188454 madgraphpythia auet2bcteq6l1 dmv dm50 mm100 w8pi qcut600
946 v06
947 mc12 188439 madgraphpythia auet2bcteq6l1 dmv dm50 mm300 w8pi qcut200
948 v06
949 mc12 188447 madgraphpythia auet2bcteq6l1 dmv dm50 mm300 w8pi qcut400
950 v06
951 mc12 188455 madgraphpythia auet2bcteq6l1 dmv dm50 mm300 w8pi qcut600
952 v06
```

```
953 mc12 188440 madgraphpythia auet2bcteq6l1 dmv dm50 mm500 w8pi qcut200  
954 v06  
955 mc12 188448 madgraphpythia auet2bcteq6l1 dmv dm50 mm500 w8pi qcut400  
956 v06  
957 mc12 188456 madgraphpythia auet2bcteq6l1 dmv dm50 mm500 w8pi qcut600  
958 v06  
959 mc12 188441 madgraphpythia auet2bcteq6l1 dmv dm50 mm1000 w8pi qcut200  
960 v06  
961 mc12 188449 madgraphpythia auet2bcteq6l1 dmv dm50 mm1000 w8pi qcut400  
962 v06  
963 mc12 188457 madgraphpythia auet2bcteq6l1 dmv dm50 mm1000 w8pi qcut600  
964 v06  
965 mc12 188442 madgraphpythia auet2bcteq6l1 dmv dm50 mm3000 w8pi qcut200  
966 v06  
967 mc12 188450 madgraphpythia auet2bcteq6l1 dmv dm50 mm3000 w8pi qcut400  
968 v06  
969 mc12 188458 madgraphpythia auet2bcteq6l1 dmv dm50 mm3000 w8pi qcut600  
970 v06  
971 mc12 188444 madgraphpythia auet2bcteq6l1 dmv dm50 mm10000 w8pi qcut200  
972 v06  
973 mc12 188452 madgraphpythia auet2bcteq6l1 dmv dm50 mm10000 w8pi qcut400  
974 v06  
975 mc12 188460 madgraphpythia auet2bcteq6l1 dmv dm50 mm10000 w8pi qcut600  
976 v06  
977 mc12 188445 madgraphpythia auet2bcteq6l1 dmv dm50 mm15000 w8pi qcut200  
978 v06  
979 mc12 188453 madgraphpythia auet2bcteq6l1 dmv dm50 mm15000 w8pi qcut400  
980 v06  
981 mc12 188461 madgraphpythia auet2bcteq6l1 dmv dm50 mm15000 w8pi qcut600  
982 v06  
983 mc12 188462 madgraphpythia auet2bcteq6l1 dmv dm400 mm500 w3 qcut200  
984 v06  
985 mc12 188468 madgraphpythia auet2bcteq6l1 dmv dm400 mm500 w3 qcut400  
986 v06  
987 mc12 188474 madgraphpythia auet2bcteq6l1 dmv dm400 mm500 w3 qcut600  
988 v06  
989 mc12 188463 madgraphpythia auet2bcteq6l1 dmv dm400 mm1000 w3 qcut200  
990 v06  
991 mc12 188469 madgraphpythia auet2bcteq6l1 dmv dm400 mm1000 w3 qcut400  
992 v06  
993 mc12 188475 madgraphpythia auet2bcteq6l1 dmv dm400 mm1000 w3 qcut600  
994 v06
```

```
995 mc12 188464 madgraphpythia auet2bcteq6l1 dmv dm400 mm3000 w3 qcut200
996 v06
997 mc12 188470 madgraphpythia auet2bcteq6l1 dmv dm400 mm3000 w3 qcut400
998 v06
999 mc12 188476 madgraphpythia auet2bcteq6l1 dmv dm400 mm3000 w3 qcut600
1000 v06
1001 mc12 188465 madgraphpythia auet2bcteq6l1 dmv dm400 mm6000 w3 qcut200
1002 v06
1003 mc12 188471 madgraphpythia auet2bcteq6l1 dmv dm400 mm6000 w3 qcut400
1004 v06
1005 mc12 188477 madgraphpythia auet2bcteq6l1 dmv dm400 mm6000 w3 qcut600
1006 v06
1007 mc12 188466 madgraphpythia auet2bcteq6l1 dmv dm400 mm10000 w3 qcut200
1008 v06
1009 mc12 188472 madgraphpythia auet2bcteq6l1 dmv dm400 mm10000 w3 qcut400
1010 v06
1011 mc12 188478 madgraphpythia auet2bcteq6l1 dmv dm400 mm10000 w3 qcut600
1012 v06
1013 mc12 188467 madgraphpythia auet2bcteq6l1 dmv dm400 mm15000 w3 qcut200
1014 v06
1015 mc12 188473 madgraphpythia auet2bcteq6l1 dmv dm400 mm15000 w3 qcut400
1016 v06
1017 mc12 188479 madgraphpythia auet2bcteq6l1 dmv dm400 mm15000 w3 qcut600
1018 v06
1019 mc12 188480 madgraphpythia auet2bcteq6l1 dmv dm400 mm500 w8pi qcut200
1020 v06
1021 mc12 188486 madgraphpythia auet2bcteq6l1 dmv dm400 mm500 w8pi qcut400
1022 v06
1023 mc12 188492 madgraphpythia auet2bcteq6l1 dmv dm400 mm500 w8pi qcut600
1024 v06
1025 mc12 188481 madgraphpythia auet2bcteq6l1 dmv dm400 mm1000 w8pi qcut200
1026 v06
1027 mc12 188487 madgraphpythia auet2bcteq6l1 dmv dm400 mm1000 w8pi qcut400
1028 v06
1029 mc12 188493 madgraphpythia auet2bcteq6l1 dmv dm400 mm1000 w8pi qcut600
1030 v06
1031 mc12 188482 madgraphpythia auet2bcteq6l1 dmv dm400 mm3000 w8pi qcut200
1032 v06
1033 mc12 188488 madgraphpythia auet2bcteq6l1 dmv dm400 mm3000 w8pi qcut400
1034 v06
1035 mc12 188494 madgraphpythia auet2bcteq6l1 dmv dm400 mm3000 w8pi qcut600
1036 v06
```

```
1037 mc12 188483 madgraphpythia auet2bcteq6l1 dmv dm400 mm6000 w8pi qcut200  
1038 v06  
1039 mc12 188489 madgraphpythia auet2bcteq6l1 dmv dm400 mm6000 w8pi qcut400  
1040 v06  
1041 mc12 188495 madgraphpythia auet2bcteq6l1 dmv dm400 mm6000 w8pi qcut600  
1042 v06  
1043 mc12 188484 madgraphpythia auet2bcteq6l1 dmv dm400 mm10000 w8pi qcut200  
1044 v06  
1045 mc12 188490 madgraphpythia auet2bcteq6l1 dmv dm400 mm10000 w8pi qcut400  
1046 v06  
1047 mc12 188496 madgraphpythia auet2bcteq6l1 dmv dm400 mm10000 w8pi qcut600  
1048 v06  
1049 mc12 188485 madgraphpythia auet2bcteq6l1 dmv dm400 mm15000 w8pi qcut200  
1050 v06  
1051 mc12 188491 madgraphpythia auet2bcteq6l1 dmv dm400 mm15000 w8pi qcut400  
1052 v06  
1053 mc12 188497 madgraphpythia auet2bcteq6l1 dmv dm400 mm15000 w8pi qcut600  
1054 v06
```

Bibliography

- 1057 [1] Collaboration ATLAS. Letter of Intent for the Phase-II Upgrade of the
1058 ATLAS Experiment. Dec 2012. URL [https://cds.cern.ch/record/](https://cds.cern.ch/record/1502664/)
1059 1502664/. Cited on pages 1, 17, 26, and 28.
- 1060 [2] B.H. Bransden and C.J. Joachain. *Quantum mechanics*. Pearson Education,
1061 second edition, 2000. Cited on page 3.
- 1062 [3] Sven-Patrik Hallsjö. Covering the sphere with noncontextuality inequal-
1063 ities. Bachelor's thesis, Linköping University, The Institute of Technol-
1064 ogy, 2013. URL [http://urn.kb.se/resolve?urn=urn:nbn:se:liu:](http://urn.kb.se/resolve?urn=urn:nbn:se:liu:diva-103663)
1065 diva-103663. Cited on page 3.
- 1066 [4] A. Zee. *Quantum Field Theory in a Nutshell*. Princeton University Press,
1067 illustrated edition edition, March 2003. ISBN 0691010196. Cited on pages
1068 3, 6, and 7.
- 1069 [5] Herbert Goldstein, Charles P. Poole, and John L. Safko. *Classical Mechanics*
1070 (*3rd Edition*). Addison-Wesley, 3 edition, June 2001. ISBN 0201657023.
1071 Cited on page 3.
- 1072 [6] W. E. Burcham and M. Jobes. *Nuclear and Particle Physics*. Pearson edu-
1073 cation, second edition, 1995. Cited on page 4.
- 1074 [7] The ATLAS Collaboration. Observation of a new particle in the search
1075 for the Standard Model Higgs boson with the ATLAS detector at the LHC.
1076 *Phys. Lett. B*, 716(arXiv:1207.7214). CERN-PH-EP-2012-218):1–29. 39 p,
1077 Aug 2012. Cited on page 4.
- 1078 [8] Standard model of elementary particles. [http://en.wikipedia.org/](http://en.wikipedia.org/wiki/File:Standard_Model_of_Elementary_Particles.svg)
1079 [wiki/File:Standard_Model_of_Elementary_Particles.svg](http://en.wikipedia.org/wiki/File:Standard_Model_of_Elementary_Particles.svg),
1080 2014. Accessed: 2014-03-24. Cited on page 4.
- 1081 [9] G. Jungman, M. Kamionkowski, and K. Griest. Supersymmetric dark matter.
1082 *Physics Reports*, 267:195–373, March 1996. doi: 10.1016/0370-1573(95)
1083 00058-5. Cited on pages 4 and 5.

- 1084 [10] NASA. NASA's solar system exploration: the planets: orbits and
1085 physical characteristics. <https://solarsystem.nasa.gov/planets/>
1086 charchart.cfm, 2014. Accessed: 2014-03-21. Cited on page 6.
- 1087 [11] T. S. van Albada, J. N. Bahcall, K. Begeman, and R. Sancisi. Distribution
1088 of dark matter in the spiral galaxy NGC 3198. *Astrophysical Journal*, 295:
1089 305–313, August 1985. doi: 10.1086/163375. Cited on page 6.
- 1090 [12] Jessica Goodman, Masahiro Ibe, Arvind Rajaraman, William Shepherd,
1091 Tim M.P. Tait, et al. Constraints on Light Majorana dark Matter from Colliders.
1092 *Phys.Lett.*, B695:185–188, 2011. doi: 10.1016/j.physletb.2010.11.009.
1093 Cited on pages 5 and 7.
- 1094 [13] ATLAS Collaboration. Search for dark matter candidates and large extra di-
1095 mensions in events with a jet and missing transverse momentum with the at-
1096 las detector. *J. High Energy Phys.*, 04(arXiv:1210.4491. CERN-PH-EP-2012-
1097 210):075. 58 p, October 2012. URL [http://cds.cern.ch/record/](http://cds.cern.ch/record/1485031)
1098 1485031. Cited on pages 5, 8, and 9.
- 1099 [14] J. Goodman, M. Ibe, A. Rajaraman, W. Shepherd, T. M. P. Tait, and H.-B. Yu.
1100 Constraints on dark matter from colliders. *Phys.Rev.D82:116010,2010*, 82
1101 (11):116010, December 2010. doi: 10.1103/PhysRevD.82.116010. Cited on
1102 page 7.
- 1103 [15] ATLAS. Atlas luminosity public results. <https://twiki.cern.ch/twiki/bin/view/AtlasPublic/LuminosityPublicResults>, 2013.
1104 Accessed: 2014-03-06. Cited on page 10.
- 1106 [16] AC Team. The four main LHC experiments, Jun 1999. URL <http://cds.cern.ch/record/40525>. Cited on page 10.
- 1108 [17] Werner Herr and B Muratori. Concept of luminosity. 2006. URL <http://cds.cern.ch/record/941318/>. Cited on page 11.
- 1110 [18] The ATLAS Collaboration. The atlas experiment at the cern large hadron col-
1111 linder. *Journal of Instrumentation*, 3(08):S08003. 437 p, 2008. URL <https://cdsweb.cern.ch/record/1129811/>. Cited on pages 11 and 12.
- 1113 [19] Joao Pequenao. Computer generated image of the whole ATLAS detector,
1114 Mar 2008. URL <http://cds.cern.ch/record/1095924>. Cited on page
1115 12.
- 1116 [20] ATLAS Collaboration. Event display for one of the monojet candidates in
1117 the data. The event has a jet with $\text{pt} = 602 \text{ GeV}$ at $\eta = -1$ and $\phi =$
1118 2.6 , $\text{MET} = 523 \text{ GeV}$, and no additional jet with $\text{pt}_{\text{jet}} > 30 \text{ GeV}$ in the fi-
1119 nal state.. [https://atlas.web.cern.ch/Atlas/GROUPS/PHYSICS/](https://atlas.web.cern.ch/Atlas/GROUPS/PHYSICS/CONFNOTES/ATLAS-CONF-2011-096/fig_08.png)
1120 [CONFNOTES/ATLAS-CONF-2011-096/fig_08.png](https://atlas.web.cern.ch/Atlas/GROUPS/PHYSICS/CONFNOTES/ATLAS-CONF-2011-096/fig_08.png), 2011. Accessed:
1121 2014-03-28. Cited on page 13.
- 1122 [21] ATLAS Collaboration. Physics at a High-Luminosity LHC with ATLAS. Jul

- 1123 2013. URL <https://cds.cern.ch/record/1564937>. Cited on page
1124 15.
- 1125 [22] J. Alwall, M. Herquet, F. Maltoni, O. Mattelaer, and T. Stelzer. MadGraph
1126 5: going beyond. *Journal of High Energy Physics*, 6:128, June 2011. doi:
1127 10.1007/JHEP06(2011)128. Cited on pages 15 and 33.
- 1128 [23] Torbjörn Sjöstrand, Stephen Mrenna, and Peter Skands. A brief introduc-
1129 tion to {PYTHIA} 8.1. *Computer Physics Communications*, 178(11):852 –
1130 867, 2008. ISSN 0010-4655. doi: [http://dx.doi.org/10.1016/j.cpc.2008.
1131 01.036](http://dx.doi.org/10.1016/j.cpc.2008.01.036). URL [http://www.sciencedirect.com/science/article/
1132 pii/S0010465508000441](http://www.sciencedirect.com/science/article/pii/S0010465508000441). Cited on pages 15 and 33.
- 1133 [24] The ROOT Team. Root. <http://root.cern.ch/drupal/>, 2014. Ac-
1134 cessed: 2014-03-28. Cited on page 15.
- 1135 [25] S. Agostinelli, J. Allison, K. Amako, J. Apostolakis, H. Araujo, P. Arce,
1136 M. Asai, D. Axen, S. Banerjee, G. Barrand, F. Behner, L. Bellagamba,
1137 J. Boudreau, L. Broglia, A. Brunengo, H. Burkhardt, S. Chauvie, J. Chuma,
1138 R. Chytracek, G. Cooperman, G. Cosmo, P. Degtyarenko, A. Dell'Acqua,
1139 G. Depaola, D. Dietrich, R. Enami, A. Feliciello, C. Ferguson, H. Fe-
1140 sefeldt, G. Folger, F. Foppiano, A. Forti, S. Garelli, S. Giani, R. Gi-
1141 annitrapani, D. Gibin, J.J. Gómez Cadenas, I. González, G. Gracia
1142 Abril, G. Greeniaus, W. Greiner, V. Grichine, A. Grossheim, S. Guatelli,
1143 P. Gumligner, R. Hamatsu, K. Hashimoto, H. Hasui, A. Heikkinen,
1144 A. Howard, V. Ivanchenko, A. Johnson, F.W. Jones, J. Kallenbach, N. Kanaya,
1145 M. Kawabata, Y. Kawabata, M. Kawaguti, S. Kelner, P. Kent, A. Kimura,
1146 T. Kodama, R. Kokoulin, M. Kossov, H. Kurashige, E. Lamanna, T. Lampén,
1147 V. Lara, V. Lefebure, F. Lei, M. Liendl, W. Lockman, F. Longo, S. Magni,
1148 M. Maire, E. Medernach, K. Minamimoto, P. Mora de Freitas, Y. Morita,
1149 K. Murakami, M. Nagamatu, R. Nartallo, P. Nieminen, T. Nishimura, K. Oht-
1150 subo, M. Okamura, S. O'Neale, Y. Oohata, K. Paech, J. Perl, A. Pfeiffer,
1151 M.G. Pia, F. Ranjard, A. Rybin, S. Sadilov, E. Di Salvo, G. Santin, T. Sasaki,
1152 N. Savvas, Y. Sawada, S. Scherer, S. Sei, V. Sirotenko, D. Smith, N. Starkov,
1153 H. Stoecker, J. Sulkimo, M. Takahata, S. Tanaka, E. Tcherniaev, E. Safai
1154 Tehrani, M. Tropeano, P. Truscott, H. Uno, L. Urban, P. Urban, M. Verderi,
1155 A. Walkden, W. Wander, H. Weber, J.P. Wellisch, T. Wenaus, D.C. Williams,
1156 D. Wright, T. Yamada, H. Yoshida, and D. Zschiesche. Geant4—a sim-
1157 ulation toolkit. *Nuclear Instruments and Methods in Physics Research*
1158 *Section A: Accelerators, Spectrometers, Detectors and Associated Equip-
1159 ment*, 506(3):250 – 303, 2003. ISSN 0168-9002. doi: [http://dx.doi.org/
1160 10.1016/S0168-9002\(03\)01368-8](http://dx.doi.org/10.1016/S0168-9002(03)01368-8). URL <http://www.sciencedirect.com/science/article/pii/S0168900203013688>. Cited on page 17.
- 1161 [26] ATLAS Collaboration. Performance assumptions for an upgraded ATLAS
1162 detector at a High-Luminosity LHC. Mar 2013. URL [https://cds.cern.
1163 ch/record/1527529/](https://cds.cern.ch/record/1527529/). Cited on pages 17, 20, 26, 27, and 28.
- 1164 [27] ATLAS Collaboration. Electron performance measurements with the ATLAS

1166 detector using the 2010 LHC proton-proton collision data. *Eur. Phys. J. C*,
1167 72(arXiv:1110.3174. CERN-PH-EP-2011-117):1909. 45 p, Oct 2011. Com-
1168 ments: 33 pages plus author list (45 pages total), 24 figures, 12 tables, sub-
1169 mitted to Eur. Phys. J. C. Cited on pages 26 and 28.

1170 [28] ATLAS Collaboration. Search for New Phenomena in Monojet plus Missing
1171 Transverse Momentum Final States using 10fb-1 of pp Collisions at $\sqrt{s}=8$
1172 TeV with the ATLAS detector at the LHC. Nov 2012. URL [http://cds.
1173 cern.ch/record/1493486/](http://cds.cern.ch/record/1493486/). Cited on pages 32, 33, 34, 36, and 37.

1174 [29] Donald Duck. The history of automatic control. *Duckburg Journal of Sci-
1175 ence*, 106(3):345–401, 2005. Cited on page 46.

1177 **Upphovsrätt**

1178 Detta dokument hålls tillgängligt på Internet — eller dess framtida ersättare —
 1179 under 25 år från publiceringsdatum under förutsättning att inga extraordinära
 1180 omständigheter uppstår.

1181 Tillgång till dokumentet innebär tillstånd för var och en att läsa, ladda ner,
 1182 skriva ut enstaka kopior för enskilt bruk och att använda det oförändrat för icke-
 1183 kommersiell forskning och för undervisning. Överföring av upphovsrätten vid
 1184 en senare tidpunkt kan inte upphäva detta tillstånd. All annan användning av
 1185 dokumentet kräver upphovsmannens medgivande. För att garantera äktheten,
 1186 säkerheten och tillgängligheten finns det lösningar av teknisk och administrativ
 1187 art.

1188 Upphovsmannens ideella rätt innehåller rätt att bli nämnd som upphovsman
 1189 i den omfattning som god sed kräver vid användning av dokumentet på ovan
 1190 beskrivna sätt samt skydd mot att dokumentet ändras eller presenteras i sådan
 1191 form eller i sådant sammanhang som är kränkande för upphovsmannens litterära
 1192 eller konstnärliga anseende eller egenart.

1193 För ytterligare information om Linköping University Electronic Press se för-
 1194 lagets hemsida <http://www.ep.liu.se/>

1195 **Copyright**

1196 The publishers will keep this document online on the Internet — or its possi-
 1197 ble replacement — for a period of 25 years from the date of publication barring
 1198 exceptional circumstances.

1199 The online availability of the document implies a permanent permission for
 1200 anyone to read, to download, to print out single copies for his/her own use and
 1201 to use it unchanged for any non-commercial research and educational purpose.
 1202 Subsequent transfers of copyright cannot revoke this permission. All other uses
 1203 of the document are conditional on the consent of the copyright owner. The
 1204 publisher has taken technical and administrative measures to assure authenticity,
 1205 security and accessibility.

1206 According to intellectual property law the author has the right to be men-
 1207 tioned when his/her work is accessed as described above and to be protected
 1208 against infringement.

1209 For additional information about the Linköping University Electronic Press
 1210 and its procedures for publication and for assurance of document integrity, please
 1211 refer to its www home page: <http://www.ep.liu.se/>